Molecular Cell

Article

Hexokinase 1 forms rings that regulate mitochondrial fission during energy stress

Graphical abstract

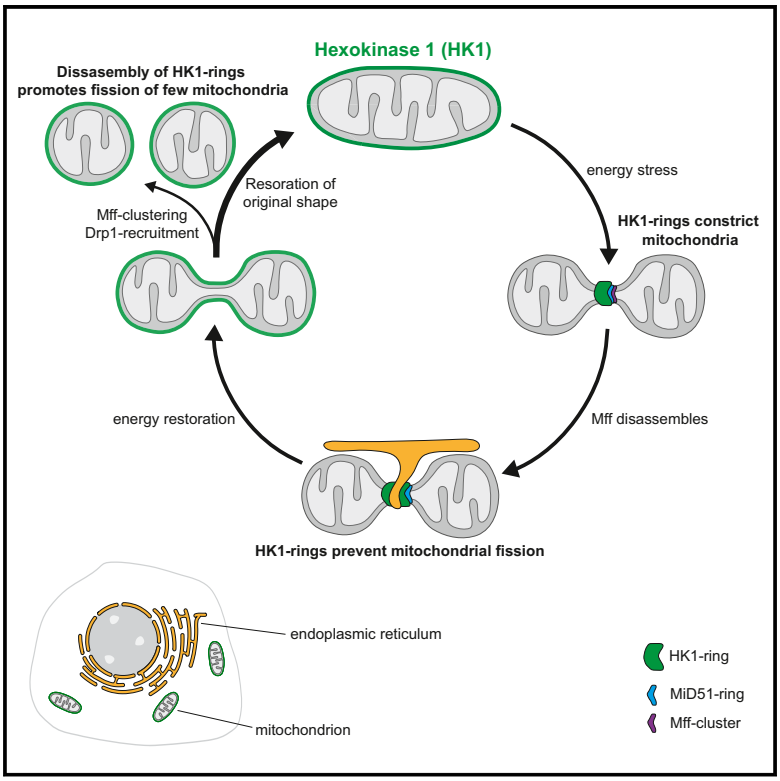

Highlights

- HK1 forms ring-like structures around mitochondria during energy stress
- HK1-rings constrict mitochondria at ER contact sites
- HK1-rings facilitate metabolic rewiring toward glutaminolysis
- HK1-rings prevent mitochondrial fission by displacing Drp1 from mitochondria

Authors

Johannes Pilic, Benjamin Gottschalk, Benjamin Bourgeois, ..., Tobias Madl, Wolfgang F. Graier, Roland Malli

Correspondence

roland.malli@medunigraz.at

In brief

Pilic et al. describe an unexpected function of hexokinase (HK1) in forming rings that constrict mitochondria during energy stress. The assembly and disassembly of HK1-rings regulates mitochondrial fission, highlighting the versatility of metabolic enzymes and the intricate interplay between cellular metabolism and organelle dynamics.

Pilic et al., 2024, Molecular Cell *84*, 1–15
July 25, 2024
https://doi.org/10.1016/j.molcel.2024.06.009

CellPress

Please cite this article in press as: Pilic et al., Hexokinase 1 forms rings that regulate mitochondrial fission during energy stress, Molecular Cell (2024), https://doi.org/10.1016/j.molcel.2024.06.009

Molecular Cell

CellPress
OPEN ACCESS

Article

Hexokinase 1 forms rings that regulate mitochondrial fission during energy stress

Johannes Pilic,[1] Benjamin Gottschalk,[1] Benjamin Bourgeois,[2,3] Hansjörg Habisch,[3] Zhanat Koshenov,[1] Furkan E. Oflaz,[1] Yusuf C. Erdogan,[1] Seyed M. Miri,[4,5] Esra N. Yiğit,[4,6] Mehmet Ş. Aydın,[4] Gürkan Öztürk,[4] Emrah Eroglu,[4,6] Varda Shoshan-Barmatz,[7] Tobias Madl,[2,3] Wolfgang F. Graier,[1,2] and Roland Malli[1,2,8,9,*]

[1]Gottfried Schatz Research Center, Molecular Biology and Biochemistry, Medical University of Graz, Neue Stiftingtalstraße 6/4, 8010 Graz, Austria

[2]BioTechMed Graz, Mozartgasse 12/2, 8010 Graz, Austria

[3]Otto Loewi Research Center, Medical Chemistry, Medical University of Graz, 8010 Graz, Austria

[4]Regenerative and Restorative Medicine Research Center (REMER), Research Institute for Health Sciences and Technologies (SABITA), Istanbul Medipol University, 34810 Istanbul, Türkiye

[5]Molecular Biology, Genetics and Bioengineering Program, Faculty of Engineering and Natural Sciences, Sabanci University, 34956 Istanbul, Türkiye

[6]Department of Physiology, International School of Medicine, Istanbul Medipol University, 34810 Istanbul, Türkiye

[7]Department of Life Sciences and the National Institute for Biotechnology in the Negev, Ben-Gurion University of the Negev, 84105 Beer-Sheva, Israel

[8]Center for Medical Research, CF Bioimaging, Medical University of Graz, Neue Stiftingtalstraße 6/6, 8010 Graz, Austria

[9]Lead contact

*Correspondence: roland.malli@medunigraz.at

https://doi.org/10.1016/j.molcel.2024.06.009

SUMMARY

Metabolic enzymes can adapt during energy stress, but the consequences of these adaptations remain understudied. Here, we discovered that hexokinase 1 (HK1), a key glycolytic enzyme, forms rings around mitochondria during energy stress. These HK1-rings constrict mitochondria at contact sites with the endoplasmic reticulum (ER) and mitochondrial dynamics protein (MiD51). HK1-rings prevent mitochondrial fission by displacing the dynamin-related protein 1 (Drp1) from mitochondrial fission factor (Mff) and mitochondrial fission 1 protein (Fis1). The disassembly of HK1-rings during energy restoration correlated with mitochondrial fission. Mechanistically, we identified that the lack of ATP and glucose-6-phosphate (G6P) promotes the formation of HK1-rings. Mutations that affect the formation of HK1-rings showed that HK1-rings rewire cellular metabolism toward increased TCA cycle activity. Our findings highlight that HK1 is an energy stress sensor that regulates the shape, connectivity, and metabolic activity of mitochondria. Thus, the formation of HK1-rings may affect mitochondrial function in energy-stress-related pathologies.

INTRODUCTION

Enzymes are known for their catalytic activity but not for other functions. These non-catalytic functions are common. A study found that one-third of yeast enzymes had knockout phenotypes that were restored by catalytically inactive versions of the enzymes.[1] A widespread non-catalytic function is the reorganization of enzymes into reversible clusters upon nutrient starvation.[2] These clusters can form large filaments that control the flux of pathways.[3] For example, yeast glucokinase polymerizes into inactive filaments to prevent excessive glycolysis upon glucose addition.[4] Based on these findings, we reasoned that investigating enzymes during changes in substrate availability will likely uncover new non-catalytic enzyme functions.

Here, we focused on mammalian hexokinase 1 (HK1), which catalyzes the ATP-dependent phosphorylation of glucose, because the purpose of its mitochondrial localization is not entirely clear. We used live-cell imaging to see whether HK1 reorganizes during changes in glucose availability. We discovered that HK1 clusters into ring-like structures around mitochondria during glucose depletion. Using genetically encoded biosensors, we found that the formation of HK1-rings is caused by glucose-depletion-induced energy stress. We designed different variants and mutants of HK1 to determine which structural motifs are crucial for the formation of HK1-rings.

RESULTS

HK1 clusters into ring-like structures during energy stress

To test how glucose availability affects the organization of HK1, we imaged HeLa cells expressing HK1-GFP and mitoDsRed, a

Please cite this article in press as: Pilic et al., Hexokinase 1 forms rings that regulate mitochondrial fission during energy stress, Molecular Cell (2024), https://doi.org/10.1016/j.molcel.2024.06.009

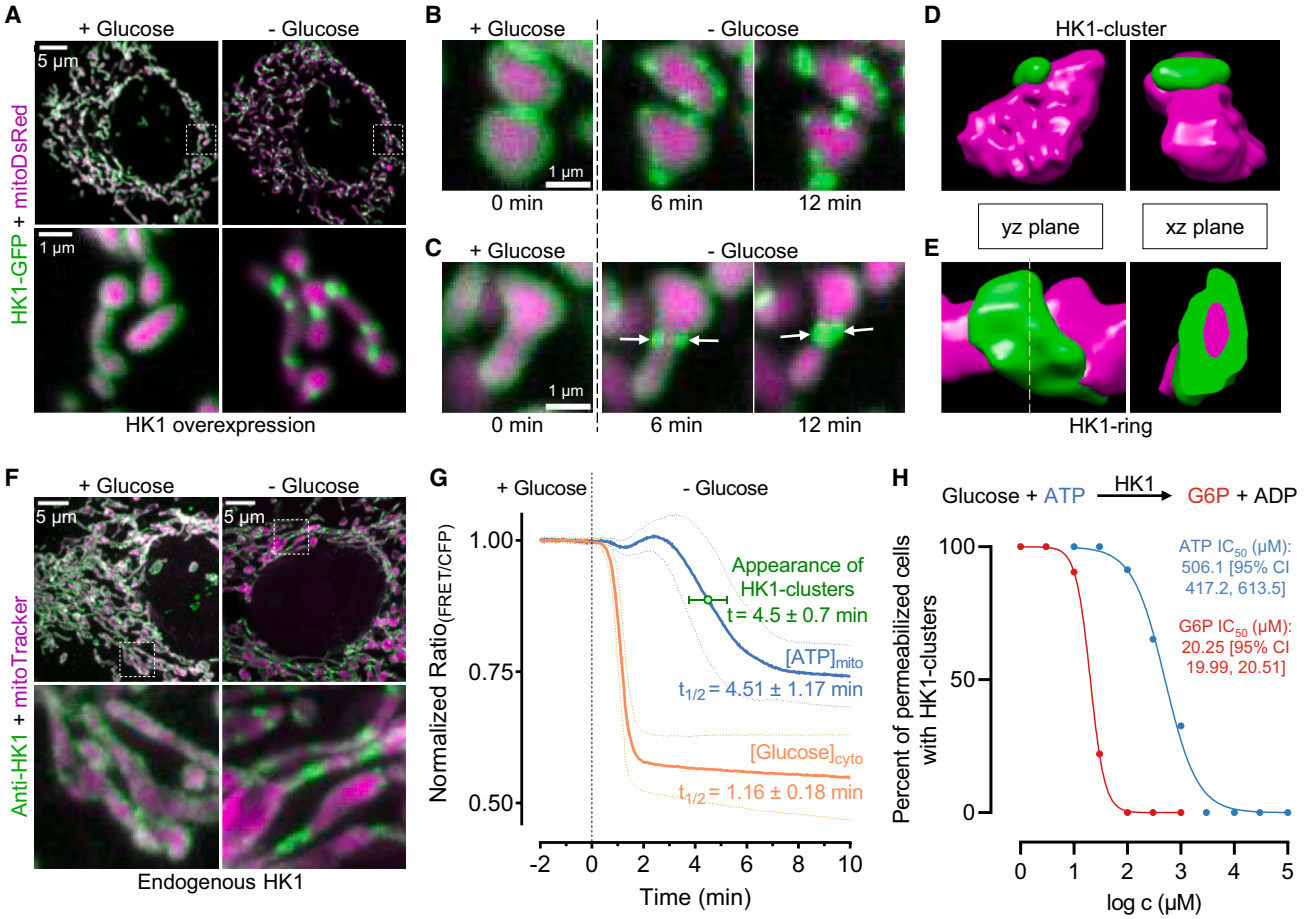

Figure 1. Hexokinase 1 clusters into ring-like structures during energy stress

(A) HK1 forms bright clusters when glucose is depleted. Confocal images of a HeLa cell expressing HK1-GFP and mitoDsRed with 10 mM glucose (left) and after 15 min of glucose depletion (right). The upper panels show an overview of the cell, and the dashed squares are magnified below.

(B and C) HK1-clusters grow in size and form ring-like structures around mitochondria. Time-lapse images of HeLa cells expressing HK1-GFP and mitoDsRed were acquired as glucose was depleted. The maturation of multiple HK1-clusters (B) or the formation of an HK1-ring (white arrows in C) is shown.

(D and E) 3D reconstructions reveal the shape of HK1-clusters and HK1-rings. Three-dimensional reconstruction of single mitochondria in HeLa cells expressing HK1-GFP and mitoDsRed. Shown are the frontal view (left) and side view (right) of an HK1-cluster (D) and an HK1-ring (E).

(F) Endogenous HK1 forms ring-like structures during glucose depletion. Immunofluorescence images of MCF-7 cells stained with anti-HK1 (green) and mitoTracker (magenta) with 10 mM glucose (left) or after 30 min of glucose depletion (right). The upper panels show an overview of the cells, and the dashed squares are magnified below.

(G) The appearance of HK1-clusters correlates more tightly with mitochondrial ATP than cytosolic glucose levels. Shown are curves of mitochondrial ATP levels (blue, $n = 123$ HeLa cells expressing mtAT1.03) and cytosolic glucose levels (orange, $n = 67$ HeLa cells expressing FLII12Pglu-700uDelta6) as glucose is depleted. Time-lapse images of HeLa cells expressing HK1-GFP were acquired at intervals of 5 s and used to assess the appearance of HK1-clusters (green, $n = 10$) as glucose is depleted. Data are presented as mean ± SD.

(H) ATP and glucose-6-phosphate (G6P) disassemble HK1-clusters in a concentration-dependent manner. The mean inhibitory effects of ATP (blue, $n = 46$ cells) and G6P (red, $n = 95$ cells) on the proportion of digitonin-permeabilized HeLa cells with HK1-clusters are shown as logarithmic concentration-response curves.

fluorescent protein targeted to the mitochondrial matrix. HK1 was distributed homogenously around mitochondria when glucose was present (Figure 1A, left images). Upon glucose depletion, HK1 formed bright clusters throughout the mitochondrial network (Figure 1A, right images and time-lapse in Video S1). Closer observations indicated that HK1-clusters grew in size (Figure 1B) and formed ring-like structures around mitochondria (Figure 1C) during glucose depletion. Three-dimensional (3D) reconstruction of z stack images revealed the shape of HK1-clusters (Figure 1D; Video S2) and that HK1 formed a closed ring around mitochondria (Figure 1E; Video S3). HK1-rings and HK1-clusters rapidly disassembled within 1.6 ± 0.3 min (mean ± SD) upon glucose readdition ($n = 10$; time-lapse in Video S4).

Because GFP fusion constructs are prone to overexpression artifacts,[5] we validated our findings with immunofluorescence. In line with the live-cell-imaging experiments using cells expressing HK1-GFP, glucose depletion also caused the formation of endogenous HK1-clusters in MCF-7 cells (Figure 1F). Next, we characterized HK1-clustering in different cell lines. HK1-clusters were present in over 90% of HK1-GFP-positive HeLa cells after

Please cite this article in press as: Pilic et al., Hexokinase 1 forms rings that regulate mitochondrial fission during energy stress, Molecular Cell (2024), https://doi.org/10.1016/j.molcel.2024.06.009

20 min of perfusion with a glucose-free buffer (Figure S1A). The proportion of cells with HK1-clusters was similar in other cell types, including neuroblastoma cells (SH-SY5Y) and mouse embryonic fibroblasts (MEFs) (Figure S1A).

However, in rat insulinoma cells (INS-1), only 7% of HK1-GFP-positive cells formed HK1-clusters after 20 min of glucose depletion (Figure S1A). Because INS-1 cells can maintain ATP levels over long periods of glucose depletion,[6] we hypothesized that HK1-clustering is caused by a lack of ATP and not by a lack of glucose. Therefore, we tested whether the appearance of HK1-clusters correlates more tightly with mitochondrial ATP than cytosolic glucose levels using genetically encoded fluorescent biosensors.[7,8] In HeLa cells, HK1-clusters appeared within 4.5 ± 0.7 min after glucose depletion, which correlated well with the drop in mitochondrial ATP with a half-time of 4.51 ± 1.17 min (Figure 1G). In contrast, cytosolic glucose levels declined rapidly after glucose depletion with a half-time of 1.16 ± 0.18 min (Figure 1G). These data point toward a link between low mitochondrial ATP levels and the formation of HK1-clusters. To further test this hypothesis, we controlled intracellular ATP and glucose levels and monitored HK1-clustering in digitonin-permeabilized HeLa cells. Permeabilization of cells with digitonin in a glucose-free buffer resulted in the formation of HK1-clusters (Figure S1B). In line with our assumption, the addition of ATP disassembled HK1-clusters in a concentration-dependent manner (Figure 1H, IC_{50} of 506.1 μM with 95% CI from 417.2 to 613.5 μM; images in Figure S1B). HK1-clusters remained stable in the presence of 10 mM glucose, indicating that glucose alone is insufficient to disassemble HK1-clusters (Figure S1C). Glucose-6-phosphate (G6P), the product of the hexokinase reaction, was more potent than ATP in reversing HK1-clustering (Figure 1H, IC_{50} of 20.25 μM with 95% CI from 19.99 to 20.51 μM; images in Figure S1D). The binding of G6P to the catalytically active site of HK1 is weakened by phosphate.[9,10] Therefore, we tested whether phosphate affects HK1-clustering when G6P is present. The addition of phosphate promoted the formation of HK1-clusters, despite the presence of G6P (Figure S1E). We next tested whether ATP-binding to HK1 is important for HK1-clustering in intact cells. We designed a GFP fusion construct of a known HK1 ATP-binding mutant (G862A) with an 11-fold lower ATP-binding affinity.[11] To induce energy stress in intact HeLa cells, glucose concentrations were gradually reduced. Cells expressing the ATP-binding mutant were approximately four times more likely to form clusters during perfusion with 0.33 mM glucose than cells expressing wild-type HK1 (Figure S1F). These data suggest that the lack of ATP promotes HK1-clustering.

Because cells likely respond to glucose depletion with autophagy and obtain energy through β-oxidation,[12] we determined whether the formation of HK1-rings is transient during prolonged glucose starvation. In HeLa cells, the HK1-rings remained stable for up to 24 h after glucose deprivation (Figure S1G).

To test the generality of our observations, we assessed the formation of HK1-rings in primary cells. HK1-rings were observed in juvenile human fibroblasts (JNHF-1), human adult epidermal keratinocytes (HEKa), human mesenchymal stem cells (hMSCs), human cerebral microvascular endothelial cells (hCMECs), and astrocytes from mouse cortical brain culture during glucose depletion (Figure S1H). HK1-rings disassembled upon glucose readdition (Figure S1H). Neurons from mouse cortical brain culture did not form HK1-rings after 20 min of glucose depletion; however, the addition of the ATP synthase inhibitor, oligomycin, led to the formation of HK1-rings (Figure S1I). In neurons, HK1-rings did not disassemble after 1 h of glucose readdition (Figure S1I). These data indicate that HK1-rings form in various cell types.

HK1-rings constrict mitochondria at ER contact sites

We observed that mitochondria are constricted at positions of HK1-rings (Figure 2A, left). To assess the degree of mitochondrial constriction, we coexpressed HK1-GFP with mitoDsRed and measured the diameter of the mitochondrial matrix at positions of HK1-rings. The diameter of the mitochondrial matrix was 0.27 ± 0.05 μm (mean ± SD) with glucose, significantly decreased to a resolution-limited minimum of 0.21 ± 0.02 μm at HK1-rings without glucose, and returned to basal levels of 0.26 ± 0.03 μm after HK1-rings disassembled upon glucose readdition (Figure 2A, right graph). Because actin contributes to the constriction of mitochondria,[13,14] we tested whether inhibition of actin polymerization with cytochalasin D before and during glucose depletion affects the formation of HK1-rings. To visualize the actin distribution relative to HK1, we coexpressed HK1-GFP with mCherry-Actin. Under basal conditions, we observed a dense network of actin fibers that disassembled upon perfusion with cytochalasin D (Figure S2A). Inhibition of actin polymerization did not affect the localization of HK1 in the presence of glucose or the formation of HK1-rings after glucose depletion (Figure S2A)., suggesting that actin is not required for the formation of HK1-rings. Next, we monitored the distribution of actin during the formation of HK1-rings using three markers: mTagBFP-Lifeact7, HK1-GFP, and mitoDsRed. We did not observe actin at sites of forming HK1-rings (Figure S2B); however, we observed dense actin cages around mitochondria during prolonged glucose depletion (Figure S2B), indicating that there is a poor temporal correlation between the formation of HK1-rings and the formation of actin cages.

We assumed that the constriction of mitochondria by HK1-rings reduces the density of cristae membranes at positions of HK1-rings. To visualize such changes in mitochondrial ultrastructure in living cells, we coexpressed HK1-GFP with ComplexIV8-mRuby2, a cristae membrane marker. Cristae membranes were absent at positions of HK1-rings (Figure 2B). To confirm the presence of mitochondrial matrix in these cristae-free regions, we additionally expressed mitoBFP, a blue fluorescent mitochondrial matrix marker (Figure S2C). Colocalization analysis confirmed that HK1-rings colocalized significantly less with the cristae membrane than with the mitochondrial matrix (Figure S2D). These data indicate that cristae membranes are displaced at positions of HK1-rings.

Because the endoplasmic reticulum (ER) is known to be involved in mitochondrial constriction,[15,16] we tested whether HK1-rings are localized at the ER using the marker BFP-KDEL. Indeed, HK1-rings colocalized with ER tubules (Figure 2C, white arrows; 3D animation in Video S5). HK1-clusters of neighboring mitochondria were frequently observed in contact (Figure S2E). ER tubules were found between HK1-cluster contact sites

Please cite this article in press as: Pilic et al., Hexokinase 1 forms rings that regulate mitochondrial fission during energy stress, Molecular Cell (2024), https://doi.org/10.1016/j.molcel.2024.06.009

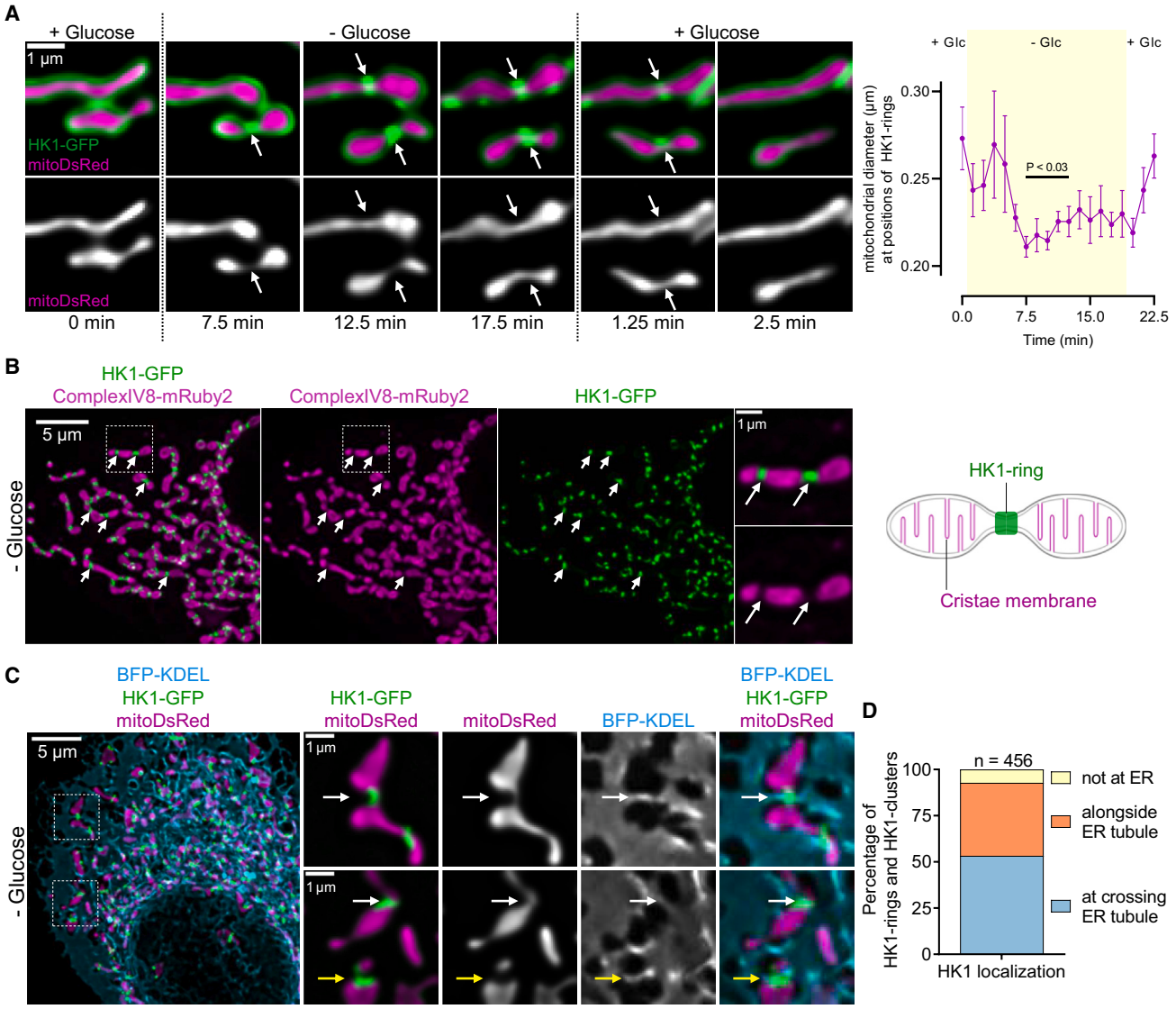

Figure 2. HK1-rings constrict mitochondria at ER contact sites

(A) HK1-rings constrict mitochondria. Time-lapse images of a HeLa cell expressing HK1-GFP and mitoDsRed were acquired as glucose was removed and re-added (left). Images are maximum intensity projections of z stacks (6 sections, spaced 0.2 µm apart). Arrows indicate sites of mitochondrial constriction at positions of HK1-rings. The diameter of the mitochondrial matrix (mean ± SEM, $n = 7$) was measured at positions of HK1-rings (right graph). The difference between basal and glucose-depleted mitochondrial diameter was evaluated using one-way ANOVA with Dunnett's post hoc test.

(B) Cristae membranes are absent at positions of HK1-rings. Confocal images of a HeLa cell expressing HK1-GFP and ComplexIV8-mRuby2 (cristae membrane) after 15 min of glucose depletion (left). Images are maximum intensity projections of z stacks (51 sections, spaced 0.2 µm apart). Arrows indicate positions of HK1-rings. Dashed squares are magnified on the right side of the overview images. Cartoon shows that cristae membranes are displaced at positions of HK1-rings (right).

(C) HK1-rings are located at ER contact sites. Confocal images of a HeLa cell expressing HK1-GFP, mitoDsRed, and BFP-KDEL (ER) after 15 min of glucose depletion. The left image shows an overview of the cell, and the dashed squares are magnified on the right side. White arrows point to positions of HK1-rings, and yellow arrows to HK1-clusters.

(D) The majority of HK1-rings and HK1-clusters are localized at the ER. Bar graph shows the percentage of HK1-rings and HK1-clusters that colocalize with the ER membrane after 15 min of glucose depletion ($n = 456$).

(Figure 2C, yellow arrows; 3D animation in Video S6). More than 90% of HK1-clusters and HK1-rings colocalized with crossing and adjacent ER tubules (Figure 2D). These data indicate that the ER is likely responsible for the positioning of HK1 during energy stress.

HK1-rings prevent mitochondrial fission during energy stress

Initially, we hypothesized that the constriction of mitochondria by HK1-rings favors mitochondrial fission. However, HeLa cells expressing HK1-GFP appeared to be protected from mitochondrial

Please cite this article in press as: Pilic et al., Hexokinase 1 forms rings that regulate mitochondrial fission during energy stress, Molecular Cell (2024), https://doi.org/10.1016/j.molcel.2024.06.009

CellPress
OPEN ACCESS

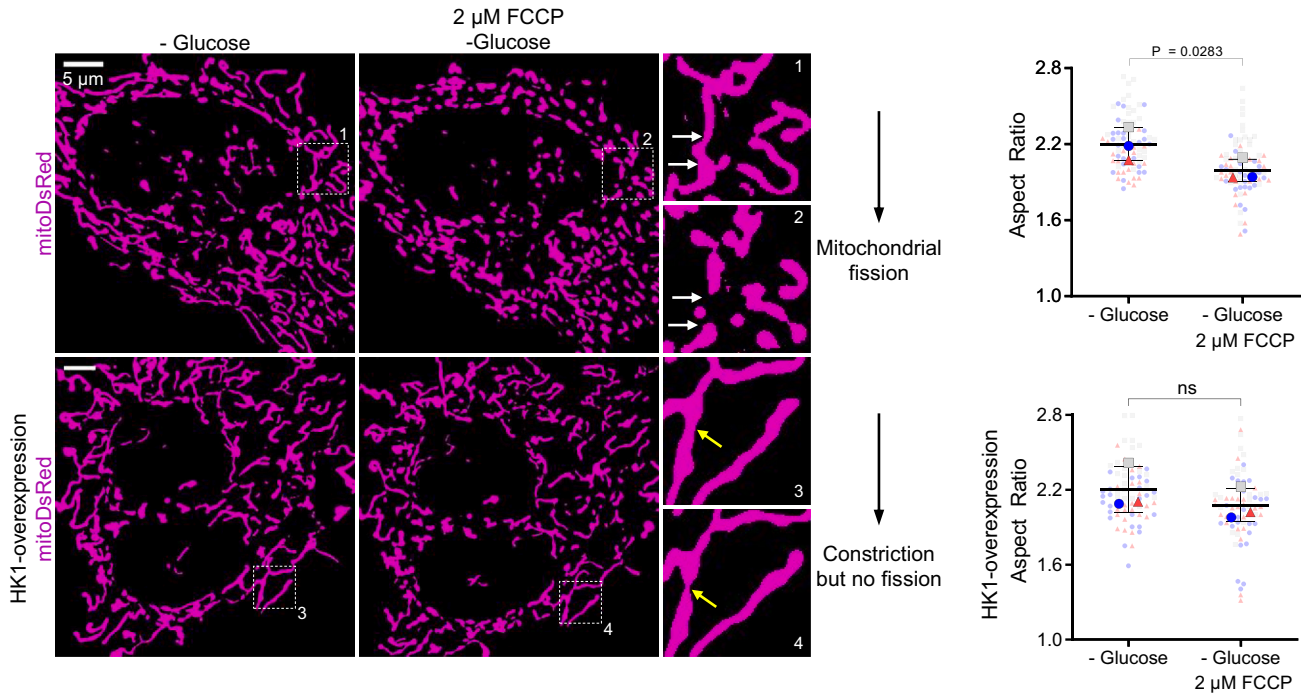

Figure 3. HK1-rings prevent mitochondrial fission during energy stress

HK1-rings prevent FCCP-induced mitochondrial fission during energy stress. Thresholded images of mitoDsRed signal in HeLa cells (top) and in HeLa cells that overexpress HK1-GFP (bottom). Glucose was depleted for 30 min before imaging (leftmost images). The middle images show the cells after perfusion with 2 μM FCCP for 20 min. Numbered dashed squares are magnified on the right side of the overview images. White arrows indicate mitochondrial fission and yellow arrows indicate mitochondrial constriction. The beeswarm SuperPlot represents each cell with a color-coded dot according to the experimental day (right). Two-tailed paired t test was used for statistical analysis (n = 3). Data are presented as mean ± SD.

fission during energy stress (Video S7). To challenge the protective effect of HK1-rings against mitochondrial fission, we compared the mitochondrial morphology of glucose-depleted HeLa cells with and without expression of HK1-GFP during perfusion with carbonyl cyanide-p-trifluoromethoxyphenylhydrazone (FCCP), a potent inducer of mitochondrial fission. Changes in mitochondrial morphology were determined with the ratio of the longest and shortest axes of a mitochondrial matrix marker (aspect ratio, AR). Low AR implies that mitochondria are fragmented, whereas high AR implies that mitochondria are elongated. As evidenced by the significant reduction in AR, FCCP treatment induced mitochondrial fission in HeLa cells that did not express HK1-GFP (Figure 3, upper). In contrast, FCCP treatment did not induce mitochondrial fission in HK1-GFP-expressing HeLa cells (Figure 3, lower). These data indicate that HK1-rings prevent FCCP-induced mitochondrial fission during energy stress.

HK1-rings displace Drp1 from mitochondria

Drp1 is a critical player in mitochondrial fission and is known to constrict mitochondria.[17] Therefore, we tested whether HK1-rings colocalized with mCherry-Drp1 and monitored their subcellular localization during glucose depletion. The number of Drp1 clusters decreased when glucose was depleted, while HK1-rings were formed (Figure 4A, images in Figure S3A). During glucose depletion, expression of HK1 significantly reduced the number of Drp1 clusters (Figure 4A, images in Figure S3A). The majority of HK1-rings and Drp1 clusters did not colocalize, and less than 20% of HK1-rings and Drp1 clusters were directly adjacent (representative image in Figure S3B, quantification in Figure S3C). Glucose readdition increased the number of Drp1 clusters while disassembling HK1-rings (Figure 4A). We found that Drp1 clustered and triggered mitochondrial fission only at a few sites where HK1-rings disassembled (Figure 4B). Next, we assessed how the different receptors for Drp1 mitochondrial fission factor (Mff), mitochondrial dynamics protein (MiD51), and mitochondrial fission 1 protein (Fis1) affect the formation of HK1-rings. For this purpose, we coexpressed mCh-Mff, mCh-MiD51, or mCh-Fis1 anchor, containing only the membrane anchor of Fis1, with HK1-GFP and assessed the percentage of cells with HK1-rings. The percentage of cells with HK1-rings was similar between control cells expressing only HK1-GFP and cells overexpressing either mCh-Mff or mCh-MiD51 in addition (Figure S3D). However, when we overexpressed the mCh-Fis1 anchor, we did not observe any cells with HK1-rings (Figure S3D), indicating that the presence of the membrane anchor of Fis1 inhibits the formation of HK1-rings. To further test the role of Fis1 in the formation of HK1-rings, we expressed HK1-mRuby3 in U2OS cells that contain endogenously tagged full-length Fis1-GFP.[18] HK1-rings displaced endogenous Fis1 during glucose depletion (Figure S3E), suggesting competitive mitochondrial interaction of Fis1 and

Please cite this article in press as: Pilic et al., Hexokinase 1 forms rings that regulate mitochondrial fission during energy stress, Molecular Cell (2024), https://doi.org/10.1016/j.molcel.2024.06.009

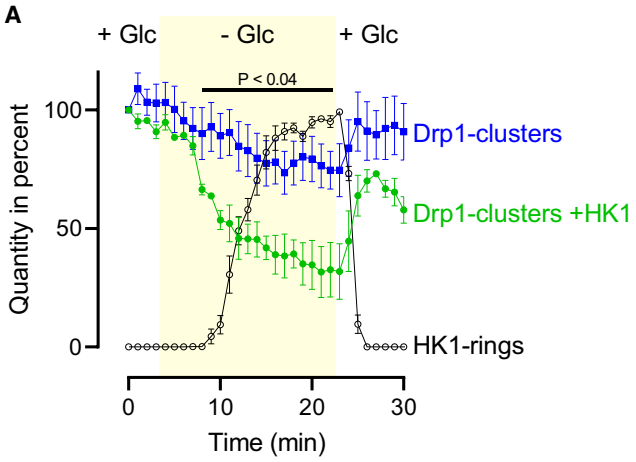

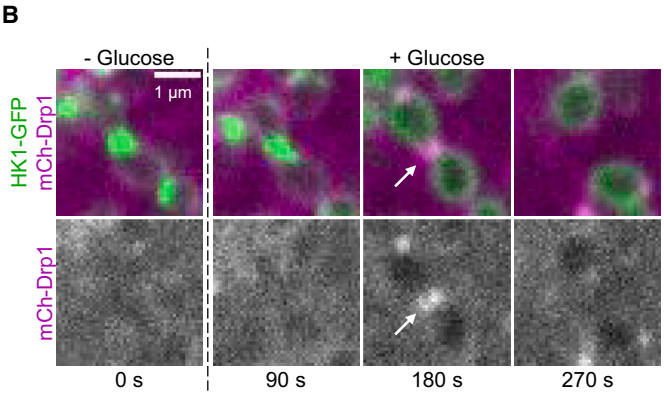

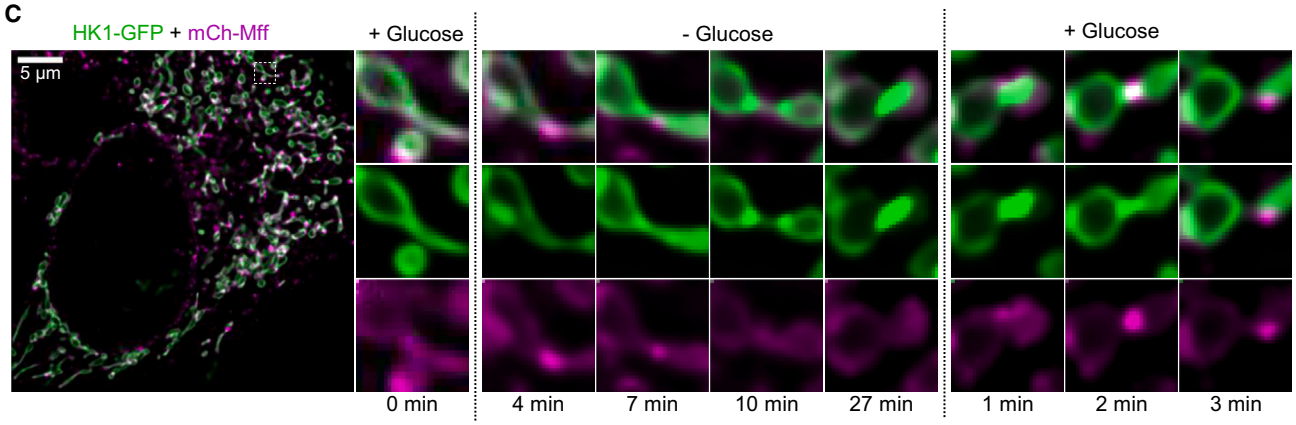

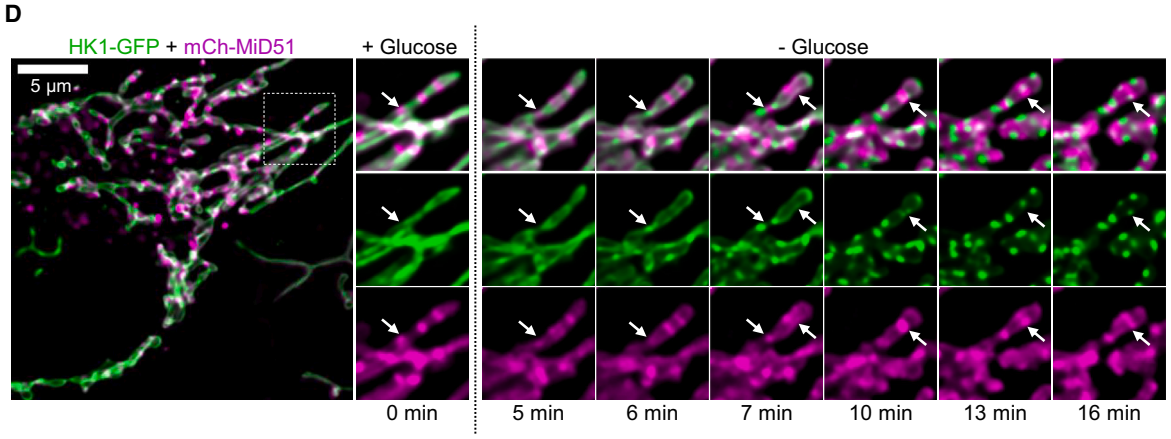

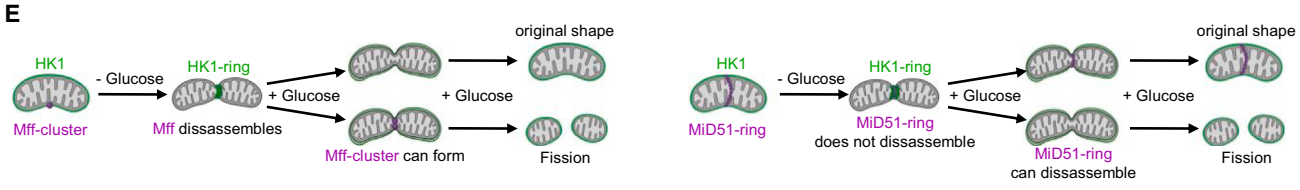

(legend on next page)

Please cite this article in press as: Pilic et al., Hexokinase 1 forms rings that regulate mitochondrial fission during energy stress, Molecular Cell (2024), https://doi.org/10.1016/j.molcel.2024.06.009

HK1-rings. Because HK1-rings appeared to be bulky structures, we tested whether the formation of HK1-rings is associated with the displacement of the other Drp1 receptors and other outer mitochondrial membrane (OMM) proteins. For this purpose, we coexpressed HK1-GFP with mCh-Mff, mCh-MiD51, or mTagBFP2-TOMM20-N-10, a marker of the OMM, and imaged their distribution during glucose depletion. HK1-rings displaced the OMM marker during glucose depletion (Figure S3F). The formation of HK1-rings during glucose depletion correlated locally and temporally with the disassembly of Mff clusters (Figure 4C). Similar to Drp1, Mff clustered and triggered mitochondrial fission only at a few sites where HK1-rings disassembled during glucose readdition (Figure 4C). We observed that HK1-rings formed at positions of MiD51 rings during glucose depletion (Figure 4D). In contrast to Mff clusters, MiD51 rings did not disassemble at the positions of HK1-rings (Figure 4D). Upon glucose readdition, MiD51 rings disassembled and triggered mitochondrial fission (Figure S3G). Based on these findings, we present a model of how glucose availability affects the interplay between HK1-rings and Mff clusters or MiD51 rings (Figure 4E). Together, our findings indicate that, at positions of bulky HK1-rings, Drp1 is unable to bind to Mff or Fis1 and carry out mitochondrial fission.

Structural features dictate the formation of HK1-clusters

We sought to identify which structural features are important for the clustering of HK1. First, we performed glucose depletion experiments with other mitochondrial hexokinases to test whether clustering is specific to HK1. HK2, which has 73% sequence homology and a similar structure to HK1, did not form clusters during glucose depletion (Figure S4A). The recently discovered HKDC1, which arose from a gene duplication event of HK1 and has 71% sequence homology to HK1,[19] showed a moderate ability to form clusters during glucose depletion (Figure S4A). These data indicate that changes in the structure of the enzyme impact the ability to form clusters.

The HK1 enzyme consists of two structurally similar halves: the catalytically inactive N-terminal and the active C-terminal half (Figure 5A). In contrast, HK2 has two catalytically active halves.[20] To identify which half is essential for HK1-clustering, we designed two chimera constructs of HK1 and HK2 fused to GFP: HK1N-HK2C and HK2N-HK1C (Figure 5B). To assess these constructs, we compared the percentage of cells that displayed cluster formation during glucose depletion. After 10 min of perfusion with a glucose-free buffer, HK1-clusters were present in 68% of cells expressing HK1-GFP. In contrast, cells expressing the HK2N-HK1C-GFP chimera did not show cluster formation under the same conditions (Figure 5B, images in Figure S4B). However, 16% of HK1N-HK2C-GFP-expressing cells showed clusters in response to glucose depletion (Figures 5B and 5C). These data demonstrate that the C-terminal half of HK1 is not essential but supports cluster formation, while the N-terminal half of HK1 is essential for cluster formation upon glucose depletion.

The N-terminal half of HK1 contains a hydrophobic mitochondrial binding domain (MBD) of 15 amino acids (Figure 5A). We tested whether truncated HK1, lacking the MBD,[21] can form clusters during glucose depletion. The truncated HK1 was localized to the cytosol and did not form clusters during glucose depletion (Figure 5D, images in Figure S4B), indicating that the MBD or a high local concentration of HK1 is needed for the formation of HK1-clusters. To assess whether the MBD alone is sufficient for clustering, we fused the MBD of HK1 to GFP (HK1MBD-GFP) and expressed the construct in HeLa cells. HK1MBD-GFP was homogeneously distributed around mitochondria and did not form clusters during glucose depletion (Figure 5D, images in Figure S4B). To test whether the MBD can accumulate at positions of HK1-rings, we imaged HK1-mRuby3 and HK1MBD-GFP in cells during glucose depletion. HK1MBD-GFP was absent at HK1-rings (Figure 5E), indicating that the MBD alone is insufficient to integrate into HK1-rings.

Next, we sought to identify which residues of the MBD are important for HK1-clustering. Therefore, we designed a chimera construct of HK1 and the MBD of HK2, HK2MBD-HK1-GFP, and monitored HK1-cluster formation during glucose depletion. The MBD of HK2 differs in residues 4, 5, 10, and 15 from the MBD of HK1 (Figure 5F). The percentage of cells with clusters was comparable in cells expressing HK2MBD-HK1-GFP and cells expressing HK1-GFP (Figure 5F, images in Figure S4C). It has been shown that replacing hydrophobic or charged residues with alanine can make membrane-curving proteins defective in their ability to tubulate membranes.[22,23] Therefore, we designed

Figure 4. HK1-rings displace Drp1 from mitochondria

(A) HK1-rings reduced the number of Drp1 clusters during energy stress. Curves show the percentage of Drp1 clusters in HeLa cells (blue) and in HeLa cells that express HK1-GFP (green) relative to the percentage of HK1-rings (black) as glucose is removed and re-added. Two-tailed unpaired t test was used for statistical analysis between Drp1 clusters and Drp1 clusters +HK1. Data are presented as mean ± SEM.

(B) HK1-ring disassembly allowed Drp1 clusters to move into constriction sites and induce mitochondrial fission. Time-lapse images of a glucose-depleted HeLa cell expressing HK1-GFP and mCherry-Drp1 were acquired at intervals of 90 s as 10 mM glucose was re-added. Arrow indicates the position of an HK1-ring.

(C) The formation of HK1-rings correlates with the disassembly of Mff clusters. Confocal images of a HeLa cell expressing HK1-GFP and mCh-Mff. The left image shows an overview of the cell in the presence of glucose, and the dashed square is magnified on the right side. Time-lapse images were acquired as glucose was removed and re-added.

(D) HK1-rings formed at sites of MiD51 rings. Confocal images of a HeLa cell expressing HK1-GFP and mCh-MiD51.The left image shows an overview of the cell in the presence of glucose, and the dashed square is magnified on the right side. Time-lapse images were acquired as glucose was removed. White arrows point to positions of HK1-rings.

(E) Model of the interplay between HK1 and Drp1 receptors. Left graph shows that during glucose depletion Mff clusters disassemble at positions of HK1-ring formation. During glucose readdition, HK1-rings disassemble and the majority of mitochondria revert to their original shape.

Only at a few mitochondria, Mff can form clusters upon disassembly of HK1-rings, triggering mitochondrial fission. The right graph shows that HK1-rings form at positions of MiD51 rings during glucose depletion. MiD51 rings do not disassemble at positions of HK1-rings. Upon glucose readdition, MiD51 ring disassembly triggers mitochondrial fission.

Please cite this article in press as: Pilic et al., Hexokinase 1 forms rings that regulate mitochondrial fission during energy stress, Molecular Cell (2024), https://doi.org/10.1016/j.molcel.2024.06.009

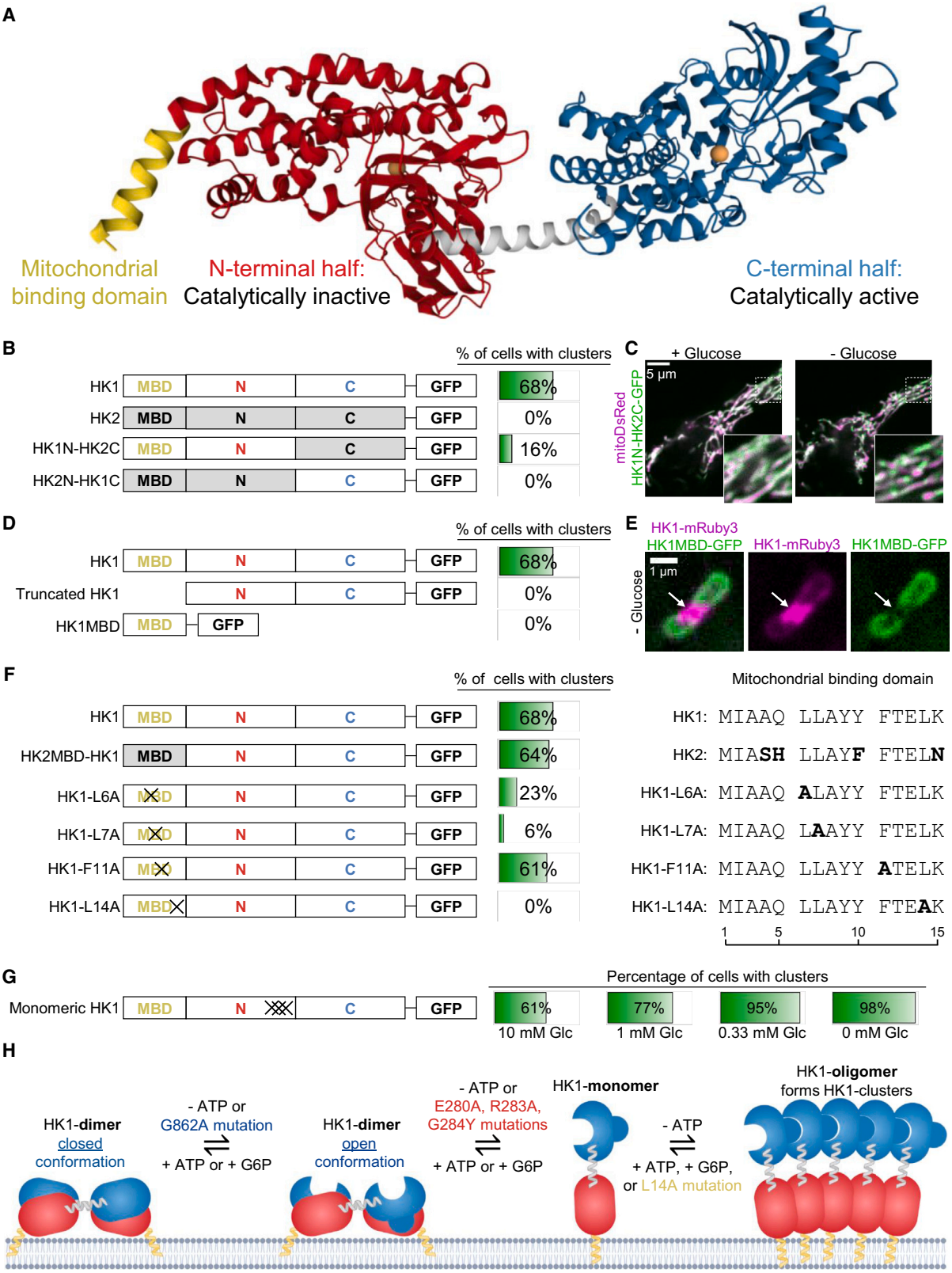

(legend on next page)

Please cite this article in press as: Pilic et al., Hexokinase 1 forms rings that regulate mitochondrial fission during energy stress, Molecular Cell (2024), https://doi.org/10.1016/j.molcel.2024.06.009

four constructs of HK1 fused to GFP with mutations in the MBD: HK1-L6A, HK1-L7A, HK1-F11A, and HK1-L14A. These mutations in the MBD did not prevent the mitochondrial localization of the constructs (Figure S4C). 61% of HK1-F11A-GFP-expressing cells, 23% of HK1-L6A-GFP-expressing cells, and only 6% of HK1-L7A-GFP-expressing cells were able to form HK1-clusters during glucose depletion (Figure 5F, images in Figure S4C). Cells expressing HK1-L14A-GFP did not show HK1-cluster formation upon glucose depletion (Figure 5F, images in Figure S4C). These data suggest that leucine residues within the MBD are crucial for the formation of HK1-clusters in response to energy stress.

Using the HK1 mutants, we challenged the protective effect of HK1-rings against mitochondrial fission by comparing the mitochondrial morphology of glucose-depleted HeLa cells expressing HK1-ATPmut-GFP, which favors ring formation, or HK1-L14A-GFP during perfusion with FCCP. FCCP treatment induced mitochondrial fragmentation in HeLa cells expressing HK1-L14A-GFP (Figure S4D, upper). In contrast, FCCP treatment did not induce mitochondrial fragmentation in HK1-ATPmut-GFP-expressing HeLa cells (Figure S4D, lower). These data indicate that single-point mutations in HK1 can alter mitochondrial dynamics during energy stress.

Because HK1 has been shown to interact with the voltage-dependent anion channel 1 (VDAC1) during its binding to mitochondria,[24] we tested whether VDAC1 localizes to HK1-rings during glucose depletion. For this purpose, we imaged HeLa cells expressing HK1-GFP and stainable tetracysteine-tagged VDAC1 (VDAC1-TC)[25] and found that HK1-rings did not colocalize with VDAC1-TC clusters during glucose depletion (Figure S4E). In addition, we tested whether the knockdown of endogenous VDAC1 affects the formation of HK1-rings. Knockdown of VDAC1 did not affect the formation of HK1-rings during energy stress (Figure S4F). These data indicate that HK1-rings form independent of VDAC1 during energy stress.

Finally, we tested whether the oligomeric state of HK1 is important for HK1-clustering. Although HK1 is monomeric in solution,[26] it is considered an oligomer of up to four subunits when bound to the OMM.[27,28] The biological significance of monomeric HK1 is unknown. Therefore, we designed a GFP fusion construct of a known monomeric HK1 triple mutant (E280A, R283A, and G284Y).[29] These mutations are located at the dimer interface and prevent dimerization of the enzyme.[29] In 61% of cells expressing monomeric HK1-GFP, clusters were found even in the presence of glucose, and glucose depletion further increased this proportion to 98% (Figure 5G, images in Figure S4G), indicating that monomeric HK1 favors the formation of HK1-clusters.

HK1-rings rewire cellular metabolism during glucose depletion

To test the functional consequences of HK1-rings formation, we focused on two established mutants, HK1-ATPmut, which favors ring formation, and HK1-L14A, which cannot form rings during energy stress. We used untargeted NMR metabolomics to examine whether HK1-rings affect cellular metabolites in glucose-starved HeLa cells. Sparse partial least-squares-discriminant analysis (sPLS-DA) was used to identify differences between non-transfected control cells and cells transfected with HK1-ATPmut or HK1-L14A. The sPLS-DA score plot demonstrates a clear separation of metabolic profiles among the three groups, with component 1 accounting for 13.2%, component 2 for 3.5%, and component 3 for 34.1% of the difference (Figure 6A, top). sPLS-DA was used to determine the most distinctive metabolites between the groups (Figure S5A). In cells transfected with HK1-ATPmut, succinate and fumarate levels were increased compared with control cells and cells transfected with HK1-L14A (Figure 6A, bottom). Importantly, under basal conditions in the presence of glucose, no increase in TCA cycle metabolites was observed in cells transfected with HK1-ATPmut (Figure S5B). To test the effects of the formation of HK1-rings on the metabolization of glutamine carbons in the TCA cycle, we performed NMR metabolomics of glucose-starved HeLa cells

Figure 5. Structural features dictate the formation of HK1-clusters

(A) X-ray structure of full-length rat HK1 (PDB: 1BG3). HK1 contains a mitochondrial binding domain (yellow), a catalytically inactive N-terminal half (red), and a catalytically active C-terminal half (blue). Glucose is shown as orange balls.

(B) The N-terminal half of HK1 is essential for the formation of HK1-clusters. Domain organization of HK1, HK2, and chimera constructs are shown on the left next to the percentages of HeLa cells with clusters after 10 min of glucose depletion. HK1 (n = 110), HK2 (n = 57), HK1N-HK2C (n = 81), and HK2N-HK1C (n = 40). MBD, mitochondrial binding domain; N, N-terminal half; C, C-terminal half.

(C) The C-terminal half of HK1 is not essential but supports cluster formation. Confocal images of a HeLa cell expressing HK1N-HK2C-GFP and mitoDsRed with 10 mM glucose (left) and after 10 min of glucose depletion (right). Dashed squares in the overview images are magnified in the bottom right corner.

(D) The MBD is necessary for the formation of HK1-clusters. Domain organization of HK1, truncated HK1, and HK1MBD are shown on the left next to the percentages of HeLa cells with clusters after 10 min of glucose depletion. HK1 (n = 110), truncated HK1 (n = 10), and HK1MBD (n = 97). MBD, mitochondrial binding domain; N, N-terminal half; C, C-terminal half.

(E) HK1MBD-GFP was absent at HK1-rings. Confocal images of a HeLa cell expressing HK1MBD-GFP and HK1-mRuby3 after 20 min of glucose depletion. Arrow indicates the position of an HK1-ring.

(F) Leucine residues within the MBD are crucial for the formation of HK1-clusters. Domain organization of HK1, HK2MBD-HK1, and mutants in the MBD are shown on the left next to the percentages of HeLa cells with clusters after 10 min of glucose depletion. HK1 (n = 110), HK2MBD-HK1 (n = 33), HK1-L6A (n = 31), HK1-L7A (n = 33), HK1-F11A (n = 28), and HK1-L14A (n = 26). Residues in the MBD of constructs that differ from HK1 are highlighted in bold (right). MBD, mitochondrial binding domain; N, N-terminal half; and C, C-terminal half. Crosses indicate mutated positions.

(G) Monomeric HK1 forms clusters even in the presence of glucose. Domain organization of monomeric HK1 (E280A, R283A, and G284Y) is shown on the left next to the percentage of HeLa cells with clusters of monomeric HK1 (n = 44) as glucose was gradually depleted in intervals of 7 min. MBD, mitochondrial binding domain; N, N-terminal half; and C, C-terminal half. Crosses indicate mutated positions.

(H) Model of HK1-clustering. Lack of ATP or mutation in the ATP-binding site favors an open conformation of the C-terminal half and is an initial step of HK1-clustering. Further depletion of ATP or mutation in the dimeric interface leads to dimer-monomer-transition. Monomeric HK1 forms new oligomers that assemble into HK1-clusters. HK1-clustering is reversed by ATP or G6P. Data are presented as mean ± SD.

Please cite this article in press as: Pilic et al., Hexokinase 1 forms rings that regulate mitochondrial fission during energy stress, Molecular Cell (2024), https://doi.org/10.1016/j.molcel.2024.06.009

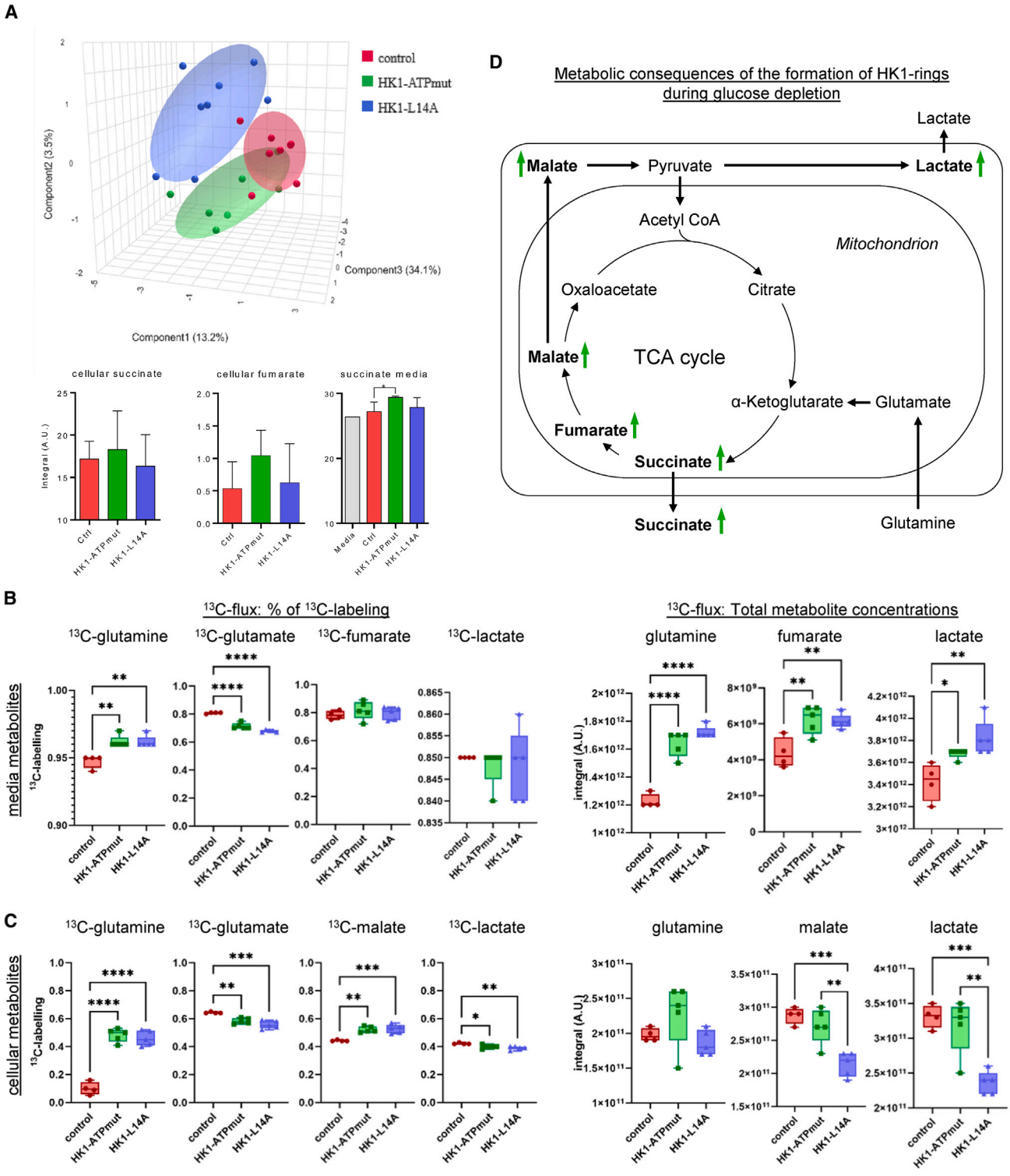

Figure 6. HK1-rings rewire cellular metabolism during glucose depletion

(A) HK1-rings affect TCA cycle metabolites. Untargeted NMR metabolomics sPLS-DA 3D score plot (top): component 1 of 13.2%, component 2 of 3.5%, and component 3 of 34.1%. Graphs show changes in the integral area of selected TCA cycle metabolites (bottom). One-way ANOVA was used for statistical analysis with Tukey post hoc analysis. Data are presented as mean ± SD.

(legend continued on next page)

Please cite this article in press as: Pilic et al., Hexokinase 1 forms rings that regulate mitochondrial fission during energy stress, Molecular Cell (2024), https://doi.org/10.1016/j.molcel.2024.06.009

that were cultured with ^{13}C-labeled glutamine. ^{13}C-glutamine was taken up and metabolized by the cells, which can be seen from the formation and release of ^{13}C-glutamate and ^{13}C-fumarate into the cell supernatant (Figure 6B, left). Intracellularly, ^{13}C-glutamine is metabolized to ^{13}C-glutamate and introduced into the TCA cycle, as reflected by the formation of ^{13}C-malate (Figure 6C, left). Interestingly, both mutants had similar effects on ^{13}C-glutamine uptake, which seemed to decrease (Figure 6B, left). Strikingly, and in line with the decreased secretion of ^{13}C-glutamate, the ^{13}C labeling of intracellular glutamine increased (Figures 6B and 6C, left). These findings suggest that the formation of HK1-rings enhances the efficiency of glutamine conversion. In agreement, we observed increased levels of cellular malate and lactate (via malic enzyme) in cells expressing the ring-forming HK1 variant (Figure 6C, right). Therefore, these data indicate that HK1-rings favor a shift in metabolism to increased TCA cycle activity (Figure 6D).

To test how HK1-rings affect cellular bioenergetics, we assessed the ratio between oxygen consumption rate (OCR) to extracellular acidification rate (ECAR) in HeLa cells transfected with HK1-ATPmut-GFP or HK1-L14A-GFP. OCR/ECAR ratio was not affected in the presence of glucose; however, in glucose-starved conditions, HK1-ATPmut transfected cells had a significantly higher OCR/ECAR ratio compared with cells transfected with HK1-L14A (Figure S5C), indicating that the formation of HK1-rings affects cellular OCR/ECAR ratio during glucose depletion.

To understand the effects of the formation of HK1-rings on mitochondrial membrane potential, we stained HeLa cells expressing HK1-ATPmut-GFP or HK1-L14A-GFP with tetramethylrhodamine methyl ester (TMRM). During glucose depletion, the TMRM intensity decreased to similar levels in cells transfected with HK1-ATPmut or HK1-L14A (Figure S5D), suggesting that the formation of HK1-rings does not affect mitochondrial membrane potential. In HeLa cells expressing HK1-GFP, FCCP treatment in the presence of glucose did not lead to the formation of HK1-rings (Figure S5E), indicating that mitochondrial depolarization alone does not trigger the formation of HK1-rings.

DISCUSSION

Here, we discovered that HK1 forms rings that constrict mitochondria during energy stress. HK1-rings are localized at contact sites with the ER and prevent Drp1-mediated mitochondrial fission. Prevention of mitochondrial fission by HK1-rings likely preserves the integrity of mitochondria during energy stress.

Based on our findings, we present a model for the formation of HK1-clusters (Figure 5H): we propose that depletion of ATP is the first step in the formation of HK1-clusters. It is not the lack of glucose but the depletion of ATP that triggers HK1-clustering. This mechanistic insight likely explains why HK1-clustering was not discovered earlier under similar conditions. One group reported that glucose depletion did not affect the subcellular location of HK1.[30,31] This could be due to low spatial resolution or the use of cell types that can maintain ATP levels during glucose depletion.[6] Interestingly, glucose alone cannot stabilize a closed conformation of the catalytically active C-terminal half.[32] A closed conformation of the C-terminal half requires ATP or G6P,[32] which led us to believe that an open conformation of the C terminus favors HK1-clustering. Supporting this assumption, we demonstrated that a point mutation in the ATP-binding site promotes the formation of HK1-clusters. Our data also indicate that G6P inhibits HK1-clustering, likely by binding to the active site of the C-terminal half,[9] stabilizing a closed conformation.[32] Because we found that monomeric HK1 favors HK1-clustering, we propose that dimer-monomer-transition is the second step in forming HK1-clusters. However, we do not yet know whether this transition occurs and whether it is necessary for the HK1-clustering. Another possibility is that the previously determined dimer interface is different from the one involved in HK1-clustering.[29] We propose that oligomerization of monomeric HK1 is the final step in HK1-clustering. We found that the N-terminal half of HK1 is essential for HK1-clustering. Although the N-terminal halves of HK1 and HK2 have similar structural folds, only the N-terminal half of HK1 can support a partially open conformation.[33] In contrast to HK1, HK2 has a catalytically active N-terminal half.[20] These structural details may explain why HK2 cannot form rings during energy stress. Our findings suggest that leucine residues within the MBD of HK1 are crucial for the formation of HK1-clusters. Although it is striking that mutations in the MBD can prevent HK1-clustering, it has been shown that mutations in membrane anchors hinder protein oligomerization by preventing tight packaging or the ability to sense curvature.[34,35] Because VDAC1 has been described to interact with HK1,[24] it was surprising that VDAC1-TC clusters did not colocalize with HK1-rings during glucose depletion. However, it is plausible that HK1 can form rings without VDAC1, as HK1 has been shown to be able to insert into the OMM, independently of VDAC1.[36,37] Collectively, our data show that HK1-clustering only occurs during cellular energy stress, defined by the depletion of ATP and G6P. Intense exercise, ischemia, and stroke have been reported to induce energy stress,[38–40] suggesting that HK1-clustering likely plays a role in these conditions. A recently developed mouse model, lacking the MBD of HK1,[41] is promising to elucidate the effects of HK1-rings in energy-stress-related conditions *in vivo*.

Our findings shed light on the potential functions of HK1-rings. We found that HK1-rings are positioned at the ER-mitochondria contact sites. These sites play crucial roles in various cellular processes, including calcium homeostasis, lipid transfer, and mitochondrial metabolism.[42] However, we do not yet know whether HK1-rings are involved in these processes or whether HK1-rings influence the communication between mitochondria and the ER during energy stress. We found that mitochondrial constriction occurred at positions of HK1-rings. Thus, HK1-rings may play a role in defining the position of mitochondrial

(B and C) HK1-rings increase TCA cycle activity. Graphs on the left side show the percentage of ^{13}C-labeling in metabolites derived from ^{13}C-glutamine, measured using NMR spectroscopy. Graphs on the right side show the total concentrations of metabolites, the concentration of metabolites are depicted in arbitrary units. One-way ANOVA was used for statistical analysis with Tukey post hoc analysis. Boxplots show median and interquartile range.
(D) Proposed model for the rewiring of cellular metabolism by HK1-rings. Green arrows indicate consequences in metabolite levels by the formation of HK1-rings.

Please cite this article in press as: Pilic et al., Hexokinase 1 forms rings that regulate mitochondrial fission during energy stress, Molecular Cell (2024), https://doi.org/10.1016/j.molcel.2024.06.009

constriction during energy stress. Actin is known to contribute to the constriction of mitochondria[13,14]; however, we found that actin polymerization is not required to form HK1-rings. HK1 and actin share structural similarities, indicating possible common ancestry.[43] Although it was assumed that HK1 had lost its ability to polymerize and generate mechanical force,[44] our findings show that HK1 polymerizes into rings that constrict mitochondria. A similar mitochondrial phenotype of constricted mitochondria, called mitochondria on a string (MOAS), has been observed in brain tissue from mice, primates, and Alzheimer's disease patients.[45–47] Interestingly, MOAS has been linked to altered energetics induced by hypoxia, hypometabolism, and aging.[45–47] We suggest that energy stress could induce this mitochondrial phenotype via the formation of HK1-rings, as it closely resembles our observations of mitochondria during energy stress. Our data also demonstrate that severe constriction of mitochondria by HK1-rings displaces the cristae membrane. Constriction of mitochondria and decreasing cristae density are the initial steps of mitochondrial fission.[13,48] However, we did not observe mitochondrial fission at HK1-rings. Instead, we found that HK1-rings prevented mitochondrial fission when mitochondria were challenged with a chemical uncoupler. The inhibition of mitochondrial fission by HK1-rings was likely caused by the inability of Drp1 to localize to Mff clusters or Fis1 at positions of HK1-rings. HK1-rings appeared to be dense structures capable of displacing OMM proteins. At a few sites of HK1-ring disassembly, we found that Mff and Drp1 could form clusters, which triggered mitochondrial fission. We found that HK1-rings colocalized with MiD51 rings. Interestingly, it has been suggested that MiD51 can sense cellular energy status and regulate mitochondrial fission.[49] Collectively, we propose that HK1-rings prevent mitochondrial fission during energy stress but likely promote fission in some mitochondria after restoration of cellular energy. The importance of promoting fission after the restoration of cellular energy remains unclear. However, inhibition of mitochondrial fission is known to reduce apoptosis and mitochondrial degradation.[50,51] Therefore, we believe that inhibition of mitochondrial fission by HK1-rings can protect against excessive fission in ischemia/reperfusion injury and heart failure.[52] We found that HK1-rings shift cellular metabolism toward increased TCA cycle activity. These alterations could be linked to the constriction of mitochondria by HK1-rings because changes in mitochondrial morphology can have a significant impact on cellular metabolism.[53] In general, fragmented mitochondrial morphology has been linked to nutrient excess, energy stress, and lipid metabolism.[54,55] For example, mitochondrial membrane curvature has been suggested to regulate fatty acid oxidation by controlling the sensitivity of carnitine palmitoyltransferase 1 to malonyl-coenzyme A (CoA).[55] Elongated mitochondrial morphology has been linked to starvation of amino acids and increased oxidative metabolism.[56,57] We have now linked the constriction of mitochondria by HK1-rings to energy stress. However, further research is needed to understand the mechanisms of how HK1-rings rewire cellular metabolism.

Limitations of the study

It remains unclear whether HK1-rings also form in living animal models during energy stress such as ischemia or stroke. Further investigation is needed to determine their physiological and pathological relevance in these contexts. It is also important to understand the long-term effects and interaction partners of HK1-rings. A further limitation of this study is that although we demonstrate that HK1-rings do not overlap with VDAC1 clusters, we do not provide additional clarification on how HK1-rings remain associated with the mitochondria. Although we could not identify the crystal structure of HK1 polymers, we predict that studying full-length HK1 without G6P and ATP has a high chance of revealing the organization of HK1-clusters. Moreover, it would be interesting to investigate the effects of HK1-rings on different metabolic pathways, e.g., fatty acid utilization in adipocytes. In addition, it would be interesting to dissect the effects of the formation of HK1-rings on mitochondrial metabolism from Drp1 activity. We do not yet know enough about the physiological and pathological relevance of our findings, but they have a wide range of implications for how HK1-rings affect mitochondrial functions during energy stress.

STAR★METHODS

Detailed methods are provided in the online version of this paper and include the following:

- KEY RESOURCES TABLE
- RESOURCE AVAILABILITY
  - Lead contact
  - Materials availability
  - Data and code availability
- EXPERIMENTAL MODEL AND STUDY PARTICIPANT DETAILS
  - Cell culture
- METHOD DETAILS
  - Transfection
  - Imaging of subcellular protein dynamics
  - Single-cell ATP and glucose imaging
  - Perfusion of cells during live cell imaging
  - Cell permeabilization
  - Chemicals
  - Mitochondrial membrane potential measurements
  - Immunofluorescence
  - VDAC1-TC labeling
  - VDAC1 knockdown and immunoblot
  - NMR metabolomic profiling
  - Seahorse measurements
- QUANTIFICATION AND STATISTICAL ANALYSIS

SUPPLEMENTAL INFORMATION

Supplemental information can be found online at https://doi.org/10.1016/j.molcel.2024.06.009.

ACKNOWLEDGMENTS

We appreciate the technical assistance from René Rost, Anna Schreilechner, Mercedes Maier, and Sinem Usluer. The research was supported by the Molecular Medicine PhD program of the Medical University of Graz and the FWF (Austrian Science Fund: I3716-B27 to R.M.). The research of T.M. was supported by Austrian Science Fund (FWF) (grants DOI: https://doi.org/10.55776/P28854, https://doi.org/10.55776/I3792, https://doi.org/10.55776/DOC130, and https://doi.org/10.55776/W1226), the Austrian Research Promotion Agency (FFG) grants 864690 and 870454, the Integrative Metabolism Research Center Graz, the Austrian Infrastructure Program 2016/2017, the Styrian Government (Zukunftsfonds, doc.fund program), the City of Graz, and BioTechMed-Graz (flagship project). For open access purposes, the

author has applied a CC BY public copyright license to any author accepted manuscript version arising from this submission. We thank Tatjana Kleele for sending us U2OS cells that endogenously express Fis1-GFP and Beate Rinner for providing us with JNHF-1 cells. We thank Emil Spreitzer for his insightful analysis. We appreciate all discussions about this work, especially with Marc Germain and Marijn Ford. We thank everyone who sent us plasmids or deposited plasmids used in this study at www.addgene.org. We are grateful to the reviewers and editors for their precious time.

AUTHOR CONTRIBUTIONS

J.P. and R.M. conceived the study. J.P., F.E.O., S.M.M., E.N.Y., M.Ş.A., and B.G. performed experiments or carried out image analysis. H.H. and T.M. carried out NMR metabolomics experiments and analyses. All authors contributed to the interpretation of results and experimental design. J.P. and R.M. wrote the first draft of the manuscript, and all authors contributed to the final version.

DECLARATION OF INTERESTS

The authors declare no competing interests.

Received: September 29, 2023
Revised: April 30, 2024
Accepted: June 11, 2024
Published: July 8, 2024

REFERENCES

1. Espinosa-Cantú, A., Ascencio, D., Herrera-Basurto, S., Xu, J., Roguev, A., Krogan, N.J., and DeLuna, A. (2018). Protein Moonlighting Revealed by Noncatalytic Phenotypes of Yeast Enzymes. Genetics *208*, 419–431. https://doi.org/10.1534/genetics.117.300377.
2. Narayanaswamy, R., Levy, M., Tsechansky, M., Stovall, G.M., O'Connell, J.D., Mirrielees, J., Ellington, A.D., and Marcotte, E.M. (2009). Widespread reorganization of metabolic enzymes into reversible assemblies upon nutrient starvation. Proc. Natl. Acad. Sci. USA *106*, 10147–10152. https://doi.org/10.1073/pnas.0812771106.
3. Park, C.K., and Horton, N.C. (2019). Structures, functions, and mechanisms of filament forming enzymes: a renaissance of enzyme filamentation. Biophys. Rev. *11*, 927–994. https://doi.org/10.1007/s12551-019-00602-6.
4. Stoddard, P.R., Lynch, E.M., Farrell, D.P., Dosey, A.M., DiMaio, F., Williams, T.A., Kollman, J.M., Murray, A.W., and Garner, E.C. (2020). Polymerization in the actin ATPase clan regulates hexokinase activity in yeast. Science. *367*, 1039–1042. https://doi.org/10.1126/science.aay5359.
5. Moore, I., and Murphy, A. (2009). Validating the location of fluorescent protein fusions in the endomembrane system. Plant Cell *21*, 1632–1636. https://doi.org/10.1105/tpc.109.068668.
6. Depaoli, M.R., Karsten, F., Madreiter-Sokolowski, C.T., Simmen, T., Graier, W.F., and Malli, R. (2018). Real-Time Imaging of Mitochondrial ATP Dynamics Reveals the Metabolic Setting of Single Cells. Cell Rep. *25*, 501–512.
7. Imamura, H., Nhat, K.P.H., Togawa, H., Saito, K., Iino, R., Kato-Yamada, Y., Nagai, T., and Noji, H. (2009). Visualization of ATP levels inside single living cells with fluorescence resonance energy transfer-based genetically encoded indicators. Proc. Natl. Acad. Sci. USA *106*, 15651–15656. https://doi.org/10.1073/pnas.0904764106.
8. Takanaga, H., Chaudhuri, B., and Frommer, W.B. (2008). GLUT1 and GLUT9 as major contributors to glucose influx in HepG2 cells identified by a high sensitivity intramolecular FRET glucose sensor. Biochim. Biophys. Acta *1778*, 1091–1099. https://doi.org/10.1016/j.bbamem.2007.11.015.
9. Fang, T.Y., Alechina, O., Aleshin, A.E., Fromm, H.J., and Honzatko, R.B. (1998). Identification of a phosphate regulatory site and a low affinity binding site for glucose 6-phosphate in the N-terminal half of human brain hexokinase. J. Biol. Chem. *273*, 19548–19553. https://doi.org/10.1074/jbc.273.31.19548.
10. Ellison, W.R., Lueck, J.D., and Fromm, H.J. (1975). Studies on the mechanism of orthophosphate regulation of bovine brain hexokinase. J. Biol. Chem. *250*, 1864–1871.
11. Zeng, C., Aleshin, A.E., Chen, G., Honzatko, R.B., and Fromm, H.J. (1998). The Roles of Glycine Residues in the ATP Binding Site of Human Brain Hexokinase. J. Biol. Chem. *273*, 700–704. https://doi.org/10.1074/jbc.273.2.700.
12. Weber, C.A., Sekar, K., Tang, J.H., Warmer, P., Sauer, U., and Weis, K. (2020). β-Oxidation and autophagy are critical energy providers during acute glucose depletion in Saccharomyces cerevisiae. Proc. Natl. Acad. Sci. USA *117*, 12239–12248. https://doi.org/10.1073/pnas.1913370117.
13. Korobova, F., Ramabhadran, V., and Higgs, H.N. (2013). An Actin-Dependent Step in Mitochondrial Fission Mediated by the ER-Associated Formin INF2. Science *339*, 464–467. https://doi.org/10.1126/science.1228360.
14. Manor, U., Bartholomew, S., Golani, G., Christenson, E., Kozlov, M., Higgs, H., Spudich, J., and Lippincott-Schwartz, J. (2015). A mitochondria-anchored isoform of the actin-nucleating spire protein regulates mitochondrial division. eLife *4*, e08828. https://doi.org/10.7554/eLife.08828.
15. Friedman, J.R., Lackner, L.L., West, M., DiBenedetto, J.R., Nunnari, J., and Voeltz, G.K. (2011). ER tubules mark sites of mitochondrial division. Science *334*, 358–362. https://doi.org/10.1126/science.1207385.
16. Nguyen, T.T., and Voeltz, G.K. (2022). An ER phospholipid hydrolase drives ER-associated mitochondrial constriction for fission and fusion. eLife *11*, e84279. https://doi.org/10.7554/eLife.84279.
17. Kraus, F., Roy, K., Pucadyil, T.J., and Ryan, M.T. (2021). Function and regulation of the divisome for mitochondrial fission. Nature *590*, 57–66. https://doi.org/10.1038/s41586-021-03214-x.
18. Kleele, T., Rey, T., Winter, J., Zaganelli, S., Mahecic, D., Perreten Lambert, H., Ruberto, F.P., Nemir, M., Wai, T., Pedrazzini, T., and Manley, S. (2021). Distinct fission signatures predict mitochondrial degradation or biogenesis. Nature *593*, 435–439. https://doi.org/10.1038/s41586-021-03510-6.
19. Irwin, D.M., and Tan, H. (2008). Molecular evolution of the vertebrate hexokinase gene family: Identification of a conserved fifth vertebrate hexokinase gene. Comp. Biochem. Physiol. Part D Genomics Proteomics *3*, 96–107. https://doi.org/10.1016/j.cbd.2007.11.002.
20. Ardehali, H., Yano, Y., Printz, R.L., Koch, S., Whitesell, R.R., May, J.M., and Granner, D.K. (1996). Functional organization of mammalian hexokinase II. Retention of catalytic and regulatory functions in both the NH2- and COOH-terminal halves. J. Biol. Chem. *271*, 1849–1852. https://doi.org/10.1074/jbc.271.4.1849.
21. Sun, L., Shukair, S., Naik, T.J., Moazed, F., and Ardehali, H. (2008). Glucose phosphorylation and mitochondrial binding are required for the protective effects of hexokinases I and II. Mol. Cell. Biol. *28*, 1007–1017. https://doi.org/10.1128/MCB.00224-07.
22. Ford, M.G.J., Mills, I.G., Peter, B.J., Vallis, Y., Praefcke, G.J.K., Evans, P.R., and McMahon, H.T. (2002). Curvature of clathrin-coated pits driven by epsin. Nature *419*, 361–366. https://doi.org/10.1038/nature01020.
23. Lee, M.C.S., Orci, L., Hamamoto, S., Futai, E., Ravazzola, M., and Schekman, R. (2005). Sar1p N-terminal helix initiates membrane curvature and completes the fission of a COPII vesicle. Cell *122*, 605–617. https://doi.org/10.1016/j.cell.2005.07.025.
24. Abu-Hamad, S., Zaid, H., Israelson, A., Nahon, E., and Shoshan-Barmatz, V. (2008). Hexokinase-I protection against apoptotic cell death is mediated via interaction with the voltage-dependent anion channel-1: mapping the site of binding. J. Biol. Chem. *283*, 13482–13490. https://doi.org/10.1074/jbc.M708216200.
25. Pilic, J., Oflaz, F.E., Gottschalk, B., Erdogan, Y.C., Graier, W.F., and Malli, R. (2023). Visualizing interactions of VDAC1 in live cells using a tetracysteine tag. Preprint at bioRxiv.

26. Aleshin, A.E.E., Malfois, M., Liu, X., Kim, C.S.S., Fromm, H.J.J., Honzatko, R.B.B., Koch, M.H.H., and Svergun, D.I.I. (1999). Nonaggregating mutant of recombinant human hexokinase I exhibits wild-type kinetics and rod-like conformations in solution. Biochemistry *38*, 8359–8366. https://doi.org/10.1021/bi990523n.

27. Xie, G., and Wilson, J.E. (1990). Tetrameric structure of mitochondrially bound rat brain hexokinase: a crosslinking study. Arch. Biochem. Biophys. *276*, 285–293. https://doi.org/10.1016/0003-9861(90)90040-6.

28. Beutner, G., Rück, A., Riede, B., and Brdiczka, D. (1998). Complexes between porin, hexokinase, mitochondrial creatine kinase and adenylate translocator display properties of the permeability transition pore. Implication for regulation of permeability transition by the kinases. Biochim. Biophys. Acta *1368*, 7–18. https://doi.org/10.1016/s0005-2736(97)00175-2.

29. Aleshin, A.E., Kirby, C., Liu, X., Bourenkov, G.P., Bartunik, H.D., Fromm, H.J., and Honzatko, R.B. (2000). Crystal structures of mutant monomeric hexokinase I reveal multiple ADP binding sites and conformational changes relevant to allosteric regulation. J. Mol. Biol. *296*, 1001–1015. https://doi.org/10.1006/jmbi.1999.3494.

30. John, S., Weiss, J.N., and Ribalet, B. (2011). Subcellular localization of hexokinases I and II directs the metabolic fate of glucose. PLoS One *6*, e17674. https://doi.org/10.1371/journal.pone.0017674.

31. Calmettes, G., John, S.A.A., Weiss, J.N.N., and Ribalet, B. (2013). Hexokinase-mitochondrial interactions regulate glucose metabolism differentially in adult and neonatal cardiac myocytes. J. Gen. Physiol. *142*, 425–436. https://doi.org/10.1085/jgp.201310968.

32. Aleshin, A.E., Zeng, C., Bartunik, H.D., Fromm, H.J., and Honzatko, R.B. (1998). Regulation of hexokinase I: crystal structure of recombinant human brain hexokinase complexed with glucose and phosphate. J. Mol. Biol. *282*, 345–357. https://doi.org/10.1006/jmbi.1998.2017.

33. Aleshin, A.E., Fromm, H.J., and Honzatko, R.B. (1998). Multiple crystal forms of hexokinase I: New insights regarding conformational dynamics, subunit interactions, and membrane association. FEBS Lett. *434*, 42–46. https://doi.org/10.1016/s0014-5793(98)00952-1.

34. Melnyk, R.A., Kim, S., Curran, A.R., Engelman, D.M., Bowie, J.U., and Deber, C.M. (2004). The Affinity of GXXXG Motifs in Transmembrane Helix-Helix Interactions Is Modulated by Long-range Communication. J. Biol. Chem. *279*, 16591–16597. https://doi.org/10.1074/jbc.M313936200.

35. Wu, T., Shi, Z., and Baumgart, T. (2014). Mutations in BIN1 Associated with Centronuclear Myopathy Disrupt Membrane Remodeling by Affecting Protein Density and Oligomerization. PLoS One *9*, e93060. https://doi.org/10.1371/journal.pone.0093060.

36. Neumann, D., Bückers, J., Kastrup, L., Hell, S.W., and Jakobs, S. (2010). Two-color STED microscopy reveals different degrees of colocalization between hexokinase-I and the three human VDAC isoforms. PMC Biophys. *3*, 4. https://doi.org/10.1186/1757-5036-3-4.

37. Haloi, N., Wen, P.-C., Cheng, Q., Yang, M., Natarajan, G., Camara, A.K.S., Kwok, W.-M., and Tajkhorshid, E. (2021). Structural basis of complex formation between mitochondrial anion channel VDAC1 and Hexokinase-II. Commun. Biol. *4*, 667. https://doi.org/10.1038/s42003-021-02205-y.

38. Vargas-Mendoza, N., Angeles-Valencia, M., Morales-González, Á., Madrigal-Santillán, E.O., Morales-Martínez, M., Madrigal-Bujaidar, E., Álvarez-González, I., Gutiérrez-Salinas, J., Esquivel-Chirino, C., Chamorro-Cevallos, G., et al. (2021). Oxidative Stress, Mitochondrial Function and Adaptation to Exercise: New Perspectives in Nutrition. Life (Basel) *11*. https://doi.org/10.3390/life11111269.

39. Stanley, W.C. (2004). Myocardial energy metabolism during ischemia and the mechanisms of metabolic therapies. J. Cardiovasc. Pharmacol. Ther. *9*, S31–S45. https://doi.org/10.1177/10742484040900104.

40. Arai, K., Lok, J., Guo, S., Hayakawa, K., Xing, C., and Lo, E.H. (2011). Cellular mechanisms of neurovascular damage and repair after stroke. J. Child Neurol. *26*, 1193–1198. https://doi.org/10.1177/0883073811408610.

41. De Jesus, A., Keyhani-Nejad, F., Pusec, C.M., Goodman, L., Geier, J.A., Stoolman, J.S., Stanczyk, P.J., Nguyen, T., Xu, K., Suresh, K.V., et al. (2022). Hexokinase 1 cellular localization regulates the metabolic fate of glucose. Mol. Cell *82*, 1261–1277.e9. https://doi.org/10.1016/j.molcel.2022.02.028.

42. Sassano, M.L., Felipe-Abrio, B., and Agostinis, P. (2022). ER-mitochondria contact sites; a multifaceted factory for Ca(2+) signaling and lipid transport. Front. Cell Dev. Biol. *10*, 988014. https://doi.org/10.3389/fcell.2022.988014.

43. Bork, P., Sander, C., and Valencia, A. (1992). An ATPase domain common to prokaryotic cell cycle proteins, sugar kinases, actin, and hsp70 heat shock proteins. Proc. Natl. Acad. Sci. USA *89*, 7290–7294. https://doi.org/10.1073/pnas.89.16.7290.

44. Barry, R.M., and Gitai, Z. (2011). Self-assembling enzymes and the origins of the cytoskeleton. Curr. Opin. Microbiol. *14*, 704–711. https://doi.org/10.1016/j.mib.2011.09.015.

45. Zhang, L., Trushin, S., Christensen, T.A., Bachmeier, B.V., Gateno, B., Schroeder, A., Yao, J., Itoh, K., Sesaki, H., Poon, W.W., et al. (2016). Altered brain energetics induces mitochondrial fission arrest in Alzheimer's Disease. Sci. Rep. *6*, 18725. https://doi.org/10.1038/srep18725.

46. Morozov, Y.M., Datta, D., Paspalas, C.D., and Arnsten, A.F.T. (2017). Ultrastructural evidence for impaired mitochondrial fission in the aged rhesus monkey dorsolateral prefrontal cortex. Neurobiol. Aging *51*, 9–18. https://doi.org/10.1016/j.neurobiolaging.2016.12.001.

47. Panes, J., Nguyen, T.K.O., Gao, H., Christensen, T.A., Stojakovic, A., Trushin, S., Salisbury, J.L., Fuentealba, J., and Trushina, E. (2023). Partial Inhibition of Complex I Restores Mitochondrial Morphology and Mitochondria-ER Communication in Hippocampus of APP/PS1 Mice. Cells *12*, 1111. https://doi.org/10.3390/cells12081111.

48. Segawa, M., Wolf, D.M., Hultgren, N.W., Williams, D.S., van der Bliek, A.M., Shackelford, D.B., Liesa, M., and Shirihai, O.S. (2020). Quantification of cristae architecture reveals time-dependent characteristics of individual mitochondria. Life Sci. Alliance *3*, e201900620. https://doi.org/10.26508/lsa.201900620.

49. Bharambe, N., and Ramachandran, R. (2019). ADP-Regulated MiD51-Phospholipid Interactions Couple Cellular Bioenergetics to Mitochondrial Membrane Remodeling. Biophys. J. *116*, 371a. https://doi.org/10.1016/j.bpj.2018.11.2017.

50. Lackner, L.L., and Nunnari, J. (2010). Small molecule inhibitors of mitochondrial division: tools that translate basic biological research into medicine. Chem. Biol. *17*, 578–583. https://doi.org/10.1016/j.chembiol.2010.05.016.

51. Si, L., Fu, J., Liu, W., Hayashi, T., Mizuno, K., Hattori, S., Fujisaki, H., Onodera, S., and Ikejima, T. (2020). Silibinin-induced mitochondria fission leads to mitophagy, which attenuates silibinin-induced apoptosis in MCF-7 and MDA-MB-231 cells. Arch. Biochem. Biophys. *685*, 108284. https://doi.org/10.1016/j.abb.2020.108284.

52. Disatnik, M.H., Ferreira, J.C.B., Campos, J.C., Gomes, K.S., Dourado, P.M.M., Qi, X., and Mochly-Rosen, D. (2013). Acute Inhibition of Excessive Mitochondrial Fission After Myocardial Infarction Prevents Long-term Cardiac Dysfunction. J. Am. Heart Assoc. *2*, e000461. https://doi.org/10.1161/JAHA.113.000461.

53. Mishra, P., and Chan, D.C. (2016). Metabolic regulation of mitochondrial dynamics. J. Cell Biol. *212*, 379–387. https://doi.org/10.1083/jcb.201511036.

54. Song, J.-E., Alves, T.C., Stutz, B., Šestan-Peša, M., Kilian, N., Jin, S., Diano, S., Kibbey, R.G., and Horvath, T.L. (2021). Mitochondrial Fission Governed by Drp1 Regulates Exogenous Fatty Acid Usage and Storage in Hela Cells. Metabolites *11*, 322. https://doi.org/10.3390/metabo11050322.

55. Ngo, J., Choi, D.W., Stanley, I.A., Stiles, L., Molina, A.J.A., Chen, P.-H., Lako, A., Sung, I.C.H., Goswami, R., Kim, M.-Y., et al. (2023). Mitochondrial morphology controls fatty acid utilization by changing

CPT1 sensitivity to malonyl-CoA. EMBO J. *42*, e111901. https://doi.org/10.15252/embj.2022111901.

56. Gomes, L.C., Di Benedetto, G., and Scorrano, L. (2011). During autophagy mitochondria elongate, are spared from degradation and sustain cell viability. Nat. Cell Biol. *13*, 589–598. https://doi.org/10.1038/ncb2220.
57. Rambold, A.S., Kostelecky, B., Elia, N., and Lippincott-Schwartz, J. (2011). Tubular network formation protects mitochondria from autophagosomal degradation during nutrient starvation. Proc. Natl. Acad. Sci. USA *108*, 10190–10195. https://doi.org/10.1073/pnas.1107402108.
58. Hohmeier, H.E., Mulder, H., Chen, G., Henkel-Rieger, R., Prentki, M., and Newgard, C.B. (2000). Isolation of INS-1-derived cell lines with robust ATP-sensitive K+ channel-dependent and -independent glucose-stimulated insulin secretion. Diabetes *49*, 424–430. https://doi.org/10.2337/diabetes.49.3.424.
59. Bischof, H., Burgstaller, S., Springer, A., Matt, L., Rauter, T., Bachkönig, O.A., Schmidt, T., Groschner, K., Schindl, R., Madl, T., et al. (2021). Potassium ions promote hexokinase-II dependent glycolysis. iScience *24*, 102346. https://doi.org/10.1016/j.isci.2021.102346.
60. Ramadani-Muja, J., Gottschalk, B., Pfeil, K., Burgstaller, S., Rauter, T., Bischof, H., Waldeck-Weiermair, M., Bugger, H., Graier, W.F., and Malli, R. (2019). Visualization of Sirtuin 4 Distribution between Mitochondria and the Nucleus, Based on Bimolecular Fluorescence Self-Complementation. Cells *8*, 1583. https://doi.org/10.3390/cells8121583.
61. Waldeck-Weiermair, M., Gottschalk, B., Madreiter-Sokolowski, C.T., Ramadani-Muja, J., Ziomek, G., Klec, C., Burgstaller, S., Bischof, H., Depaoli, M.R., Eroglu, E., et al. (2019). Development and Application of Sub-Mitochondrial Targeted Ca2 + Biosensors. Front. Cell. Neurosci. *13*, 449. https://doi.org/10.3389/fncel.2019.00449.
62. Wong, Y.C., Kim, S., Cisneros, J., Molakal, C.G., Song, P., Lubbe, S.J., and Krainc, D. (2022). Mid51/Fis1 mitochondrial oligomerization complex drives lysosomal untethering and network dynamics. J. Cell Biol. *221*, e202206140. https://doi.org/10.1083/jcb.202206140.
63. Ghaffari Zaki, A., Yiğit, E.N., Aydın, M.Ş., Vatandaslar, E., Öztürk, G., and Eroglu, E. (2024). Genetically Encoded Biosensors Unveil Neuronal Injury Dynamics via Multichromatic ATP and Calcium Imaging. ACS Sens. *9*, 1261–1271. https://doi.org/10.1021/acssensors.3c02111.
64. Kreuzer, K., Reiter, A., Birkl-Töglhofer, A.M., Dalkner, N., Mörkl, S., Mairinger, M., Fleischmann, E., Fellendorf, F., Platzer, M., Lenger, M., et al. (2022). The PROVIT Study-Effects of Multispecies Probiotic Add-on Treatment on Metabolomics in Major Depressive Disorder-A Randomized, Placebo-Controlled Trial. Metabolites *12*, 770. https://doi.org/10.3390/metabo12080770.
65. Zhang, F., Kerbl-Knapp, J., Akhmetshina, A., Korbelius, M., Kuentzel, K.B., Vujić, N., Hörl, G., Paar, M., Kratky, D., Steyrer, E., and Madl, T. (2021). Tissue-Specific Landscape of Metabolic Dysregulation during Ageing. Biomolecules *11*, 235. https://doi.org/10.3390/biom11020235.

Please cite this article in press as: Pilic et al., Hexokinase 1 forms rings that regulate mitochondrial fission during energy stress, Molecular Cell (2024), https://doi.org/10.1016/j.molcel.2024.06.009

STAR★METHODS

KEY RESOURCES TABLE

REAGENT or RESOURCE	SOURCE	IDENTIFIER
Antibodies		
Hexokinase I (C35C4) Rabbit mAb	Cell Signaling Technologies	Cat# 2024S; RRID:AB_2116996
Goat anti-Rabbit IgG (H+L) Cross-Adsorbed Secondary Antibody, Alexa Fluor™ 488	Thermo Fisher Scientific	Cat# A-11008; RRID:AB_143165
Mouse Anti-VDAC1 antibody	Abcam	Cat# ab186321
Mouse Monoclonal Anti-β-Actin	Sigma-Aldrich	Cat# A5316; RRID:AB_476743
HRP-conjugated Anti-Mouse Antibody	Sigma-Aldrich	Cat# A9044; RRID:AB_258431
Bacterial and virus strains		
NEB® 5-alpha Competent *E. coli*	New England Biolabs	C2987I
Biological samples		
Primary cortical brain culture	This study	N/A
Chemicals, peptides, and recombinant proteins		
PolyJet™	SignaGen Laboratories	SL100688
ScreenFect A-plus	Screenfect GmbH	S-6001
MitoTracker Red CMXRos	Thermo Fisher Scientific	M7512
Cytochalasin D	Sigma-Aldrich	C8273
FCCP	Sigma-Aldrich	C2920
Oligomycin	Enzo Life Sciences	ALX-380-037
Critical commercial assays		
Seahorse XFe96 Extracellular Flux Assay Kit	Agilent	102416-100
Experimental models: Cell lines		
HeLa S3	ATCC	N/A
SH-SY5Y	ATCC	N/A
MCF-7	CellBank Graz	N/A
MEF (mouse embryonic fibroblasts)	Thomas Simmen, University of Alberta, Canada	N/A
INS-1 (832/13)	C. B. Newgard, Duke University School of Medicine, USA[58]	N/A
Primary Juvenile Human Skin Fibroblasts	CellBank Graz	N/A
Primary human epidermal keratinocyte (HEKa)	ATCC	PCS-200-011
Human cerebral microvascular endothelial cells (hCMEC/D3)	CELLutions BIOSYSTEMS	CLU512
U2OS Fis1 GFP	Tatjana Kleele, ETH Zürich, Switzerland	N/A
Oligonucleotides		
siVDAC1 (5'-3' ACACUAGGCACCGAGA UUA)	Microsynth	N/A
siCtrl (5'-3' UUCUCCGAACGUGUCACGU)	Microsynth	N/A
Recombinant DNA		
HK1-GFP	Sun et al.[21], Addgene	#21917
HK1-mRuby3	Bischof et al.[59]	N/A
HK1-ATPmut-GFP / (G862A)[11]	This study	N/A
Monomeric-HK1-GFP / (E280A, R283A, G284Y)[29]	This study	N/A
HKDC1-GFP	This study	N/A
HK2-GFP	Sun et al.[21], Addgene	#21920
HK1N-HK2C-GFP	This study	N/A

(*Continued on next page*)

Please cite this article in press as: Pilic et al., Hexokinase 1 forms rings that regulate mitochondrial fission during energy stress, Molecular Cell (2024), https://doi.org/10.1016/j.molcel.2024.06.009

Continued

REAGENT or RESOURCE	SOURCE	IDENTIFIER
HK2N-HK1C-GFP	This study	N/A
Truncated-HK1-GFP	Sun et al.[21], Addgene	#21918
HK1MBD-GFP	This study	N/A
HK2MBD-HK1-GFP	This study	N/A
HK1-L6A-GFP	This study	N/A
HK1-L7A-GFP	This study	N/A
HK1-F11A-GFP	This study	N/A
HK1-L14A-GFP	This study	N/A
mitoDsRed	Addgene	#44386
mito-sfGFP	Ramadani-Muja et al.[60]	N/A
mitoBFP	Addgene	#49151
ComplexIV8-mRuby2	Waldeck-Weiermair et al.[61]	N/A
BFP-KDEL	Addgene	#49150
mCherry-Actin	Addgene	#54957
mTagBFP-Lifeact-7	Addgene	#54496
mCherry-Drp1	Addgene	#49152
mCh-Fis1	Addgene	#182580
mCh-Mff	Addgene	#157760
mCh-MiD51	Wong et al.[62]	N/A
BFP-Tom20	Addgene	#55328
VDAC1-TC	Pilic et al.[25], Addgene	#211733
mtAT1.03	Imamura et al.[7]	N/A
FLII12Pglu-700uDelta6	Takanaga et al.[8], Addgene	#17866
Software and algorithms		
Fiji	http://fiji.sc	RRID:SCR_002285
Nikon NIS-Elements	https://www.nikoninstruments.com/Products/Software	RRID:SCR_014329
MetaboAnalyst 5.0	https://www.metaboanalyst.ca/	RRID:SCR_015539
GraphPad Prism9	http://www.graphpad.com/	RRID:SCR_002798

RESOURCE AVAILABILITY

Lead contact

Further information and requests for resources and reagents should be directed to and will be fulfilled by the lead contact, Roland Malli (roland.malli@medunigraz.at).

Materials availability

Plasmids generated in this study are available from the lead contact upon request.

Data and code availability

- Microscopy data reported in this paper will be shared by the lead contact upon request.
- Any additional information required to reanalyze the data reported in this paper is available from the lead contact upon request.
- This paper does not report original code.

EXPERIMENTAL MODEL AND STUDY PARTICIPANT DETAILS

Cell culture

HeLa, SH-SY5Y, MCF-7, MEF cells, and primary juvenile human skin fibroblasts (JNHF-1) were cultured in Dulbecco's modified Eagle's medium (DMEM D5523, Sigma-Aldrich) supplemented with 10% FCS, 10 mM $NaHCO_3$, 50 U/mL penicillin-streptomycin, 1.25 μg/mL amphotericin B and 25 mM HEPES; pH was adjusted to 7.45 with NaOH. For U2OS Fis1-GFP cells additional 15 mM

Please cite this article in press as: Pilic et al., Hexokinase 1 forms rings that regulate mitochondrial fission during energy stress, Molecular Cell (2024), https://doi.org/10.1016/j.molcel.2024.06.009

glucose was supplemented. INS-1 cells were cultured in RPMI 1640 medium (Gibco) supplemented with 10% FCS, 10 mM HEPES, 2 mM L-glutamine, 1 mM sodium pyruvate, 0.05 mM beta-mercaptoethanol, 50 U/mL penicillin-streptomycin, 1.25 μg/mL amphotericin B. Human mesenchymal stem cells (hMSC) were cultured in low-glucose DMEM (11885084, Gibco) supplemented with 10% FBS and 50 U/mL penicillin-streptomycin. Primary human epidermal keratinocyte (HEKa) cells were cultured in high-glucose DMEM (25200056, Gibco) supplemented with 10% FBS and 50 U/mL penicillin-streptomycin. Human cerebral microvascular endothelial cells (hCMEC/D3) were cultured in endothelial cell growth medium (Curio Biotech) supplemented with 50 U/mL penicillin-streptomycin, 1× antibiotic-antimycotic (Gibco), and 1× Normocin (Invivogen). Primary neuron cultures were performed following the protocol described as described previously.[63] To obtain primary neurons, postnatal (p0-p3) BALB/C mice were euthanized by decapitation, and their brains were subsequently collected. The experimental procedures conducted in this study were ethically approved by the Istanbul Medipol University Animal Experimentation Ethical Committee (IMU-HADYEK). The cortical tissue from both hemispheres was dissected under aseptic conditions and dipped into ice-cold L15 (A1247501, ThermoFisher Scientific) containing 1% antibiotic-antimycotic. Following dissection, the cortical tissue was subjected to papain (P4762, Sigma) at 4°C for 45 min. Subsequently, DNAse (D5025, Sigma) was added, and the tissue was subjected to mechanical trituration. The homogenized tissue was then centrifuged in additional fresh media containing 10% FBS at 180 g for 5 min, and the resulting cell pellet was plated onto poly-D-lysine-coated glass-bottom culture dishes using Neurobasal-A (10888022, Gibco) supplemented with 1% GlutaMAX (35050061, Gibco), 1% antibiotic/antimycotic, and 2% B27 (17504044, Gibco). All cells were grown in a humified atmosphere of 5% CO_2 at 37°C.

METHOD DETAILS

Transfection

Cells were seeded in 6-well plates on 30 mm glass coverslips (Paul Marienfeld GmbH & Co. KG, Lauda-Königshofen, Germany) and transfected using PolyJet (SignaGen Laboratories). Per well, 3 μl of PolyJet reagent was mixed with 1 μg of plasmid DNA in 100 μl of DMEM devoid of serum and antibiotics. The transfection mixture was added to 1 ml of culture medium for 8 h and was then replaced with 2 ml of culture medium. To transfect hMSCs, hCMEC cells, and primary neurons, 1×10^6 cells were resuspended in 100 μl of optiMEM (Gibco, 11058021) in the presence of 10 μg plasmid DNA. The mixture was then electroporated using a NEPA21 electroporator (Sonidel, Dublin, Ireland) in electroporation cuvettes with a 2-mm gap, each containing a 100 μl sample solution. The electroporation conditions included a voltage of 125 V with a 5 ms poring pulse length. The electroporated cells were then immediately seeded onto two wells of a 6-well plate (Greiner Bio-One, 657160, Austria) containing 30 mm glass coverslips No.1 (Glaswarenfabrik Karl Knecht Sondheim, Germany) and prewarmed respective media. Imaging was performed 24 - 48 h after transfection.

Imaging of subcellular protein dynamics

Before imaging, cells were put into a storage buffer, which was composed of 138 mM NaCl, 5 mM KCl, 2 mM $CaCl_2$, 1 mM $MgCl_2$, 10 mM HEPES, 2.6 mM $NaHCO_3$, 0.44 mM KH_2PO_4, 0.34 mM Na_2HPO_4, 10 mM D-glucose, 2 mM L-glutamine, 1X MEM amino, 1X MEM vitamins, 1% penicillin-streptomycin and 1% Amphotericin B; pH was adjusted to 7.45 with NaOH.

High-resolution imaging was performed with an array confocal laser scanning microscope (Axiovert 200 M, Zeiss) equipped with a 100×/1.45 NA oil immersion objective (Plan-Fluor, Zeiss) and a Nipkow-based confocal scanner unit (CSU-X1, Yokogawa Electric Corporation). Laser light of diode lasers (Visitron Systems, Pucheim, Germany) served as the excitation light source: BFP, GFP, and RFP fusion constructs were excited with 405, 488, and 561 nm lasers, respectively. Emission light was captured with a CoolSNAP HQ2 CCD Camera (Photometrics Tucson, Arizona, USA) using the emission filters ET460/50m, ET525/36m, and ET630/75m (Chroma Technology Corporation) for BFP, GFP, and RFP fusion constructs, respectively.

Imaging of hMSC, HEKa, hCMEC, and primary neuron culture was conducted using a laser scanning confocal microscope (LSM 880, Carl ZEISS) equipped with a Plan-Apochromat 100x/1.4NA oil immersion objective, 488 nm and 594 nm excitation lasers, and Airyscan detector for GFP and MitoTracker, respectively.

Super-resolution imaging was performed with a structured illumination microscope (Nikon) equipped with a 100×/1.49 NA oil immersion objective (CFI Aopchromat TIRF, Nikon), standard filter sets, and two iXon EMCCD cameras (Andor). GFP and RFP fusion constructs were excited with 488 and 561 nm lasers, respectively.

Image analysis was performed with Fiji software. Z-stack images with a step size of 200 nm were deconvoluted and background-subtracted using a rolling ball radius of 50 to 300 pixels. For colocalization analysis, ROIs were drawn around cells using the polygon tool, and the Pearson coefficient was measured using the ImageJ plugin coloc2. The width of mitochondria was measured with the full width at half maximum. The TrackMate plugin was used to quantify HK1-clusters, HK1-rings, and Drp1-clusters. To assess mitochondrial morphology, 2D images of a mitochondrial matrix marker were thresholded using the Otsu method, and the ratio of the longest and shortest axes of a mitochondrial matrix marker was calculated.

Single-cell ATP and glucose imaging

ATP and glucose FRET-imaging was performed with an inverted microscope (IX73 system, Vienna, Austria) equipped with a 40×/1.4 NA oil immersion objective (UPLXAPO40XO, Olympus) and an optical beam splitter (Photometrics DV2, Photometrics, Tucson, AZ, USA). HeLa cells expressing the mitochondria-targeted mtAT1.03 or cytosolic FLII12Pglu-700uDelta6 CFP-YFP-based biosensors

Please cite this article in press as: Pilic et al., Hexokinase 1 forms rings that regulate mitochondrial fission during energy stress, Molecular Cell (2024), https://doi.org/10.1016/j.molcel.2024.06.009

were imaged. To excite the CFP of the FRET pair, we used an LED-based light source (LEDHub, Omicron) and a 427/10 Brightline HC excitation filter (Semrock). Emission light was captured with a Retiga R1 CCD camera (Teledyne QImaging) using a CFP/YFP/mCherry triple LED HC emission filter (Semrock).

Perfusion of cells during live cell imaging

Transfected cells on 30 mm coverslips were put in a PC30 perfusion chamber (NGFI, Graz, Austria) and perfused at a flow rate of approximately 1 ml per minute with a gravity-based perfusion system (PS9, NGFI). Glucose buffer was composed of 135 mM NaCl, 5 mM KCl, 2 mM $CaCl_2$, 1 mM $MgCl_2$, 10 mM HEPES, and 10 mM D-glucose; pH was adjusted to 7.45 with NaOH. The glucose-free buffer contained 10 mM D-mannitol instead of glucose.

Cell permeabilization

Cells were perfused with 10 μM digitonin for 4 min in a buffer mimicking the intracellular ion composition. The buffer was composed of 10 mM NaCl, 110 mM KCl, 1 mM $MgCl_2$, 0.1 mM EGTA, 10 mM HEPES, and 10 mM D-glucose; pH was adjusted to 7.4 with NaOH. The glucose-free intracellular buffer contained 10 mM D-mannitol instead of glucose. For dose-response experiments, ascending levels of ATP or G6P were added to the glucose-free intracellular buffer, and the percentage of cells with HK1-clusters was assessed. For phosphate addition experiments, 100 μM G6P was added to phosphate-buffered saline (PBS).

Chemicals

To stain the inner mitochondrial membrane, cells were incubated with 200 nM MitoTracker Red CMXRos (Thermofisher) in storage buffer for 10 minutes at 37°C and washed afterward with storage buffer. To inhibit actin polymerization, cells were perfused with 10 μM cytochalasin D (Sigma) in glucose buffer. To induce mitochondrial fission, cells were perfused with 2 μM FCCP (Sigma) in glucose-free buffer. To induce energy stress in neurons, cells were perfused with 2 μM oligomycin (Enzo).

Mitochondrial membrane potential measurements

HeLa cells were incubated with 25 nM TMRM (tetramethylrhodamine methyl ester, Invitrogen) in storage buffer for 15 min at 37°C. After incubation, cells were washed with storage buffer to remove excess dye. The ratio between mitochondrial to nuclear TMRM intensity ratio was calculated and the minimum ratio was normalized to 1.

Immunofluorescence

MCF-7 cells were seeded in 6-well plates on 30 mm coverslips to reach a confluency of ~80%. Cells were then taken from the incubator and put in storage buffer containing 1 μM MitoTracker Red CMXRos for 10 min at 37°C. To induce HK1-ring formation, cells were perfused with glucose-free buffer for 30 minutes. Control cells were perfused with glucose buffer. All cells were washed twice with PBS and fixed with 4% paraformaldehyde at room temperature for 15 min. Then cells were washed 3x with PBS and blocked with 5% BSA in PBS for 1 h while mildly shaking. Then the blocking buffer was replaced with 1:1000 diluted HK1 rabbit monoclonal antibody (cell signaling, #2024) in PBS with 5% BSA. Cells were incubated with the primary antibody overnight at 4°C, mildly shaking. On the next day, primary antibody solution was removed, cells were washed 3x with PBS, and secondary antibody solution containing Alexa Fluor 488 goat anti-rabbit (Thermo Fisher Scientific) at a dilution of 1:2.500 was added. Cells were incubated for 2 h in the dark at room temperature, mildly shaking. Finally, cells were washed 3x for 5 minutes with PBS, Vectashield antifade mounting medium (Vectorlabs), and the coverslips were sealed with nail polish.

VDAC1-TC labeling

Cells expressing tetracysteine-tagged VDAC1 (VDAC1-TC) were labeled with 166 nM ReAsH-EDT_2 (Cayman chemical, Michigan USA) in storage buffer for 15 min at 37°C. The cells were washed with 100 μM BAL (British anti-Lewisite) in storage buffer for 10 min at 37°C and kept in storage buffer before confocal imaging.

VDAC1 knockdown and immunoblot

Cells were seeded in 6-well plates and transfected using SecreenFect A plus (SignaGen Laboratories). Per well, 60 pmol of siVDAC1 (Microsynth, 5'-3' ACACUAGGCACCGAGA UUA) or siCtrl (Microsynth, 5'-3' UUCUCCGAACGUGUCACGU) was mixed with 2.5 μl of ScreenFectA-plus transfection reagent (Screenfect GmbH) in dilution buffer (Screenfect GmbH). The transfection mixture was added to the cells for 8 hs, then the culture media was replaced. Imaging or protein extraction for immunoblot was performed 48 h after transfection. For immunoblot, cells were harvested with RIPA buffer (25 mM Tris-HCl, 150 mM NaCl, 5 mM EDTA, 1 % Triton X-100, 1 % sodium deoxycholate, 0.1 % SDS; pH was adjusted to 7.60 with NaOH.) supplemented with protease inhibitor cocktail (Sigma). Protein concentration of extracted proteins was determined with BCA Assay (ThermoFisher Scientific) on a CLARIOstar Plus (BMG Labtech). 30 μg protein per condition was resolved with a 12.5% SDS-polyacrylamide gel and transferred to a PVDF membrane (Merck Millipore). The membrane was blocked with 5% milk powder (Merck Millipore) in TBS-Tween (20 mM Tris, 0.14 M NaCl, 0.1% Tween-20, pH 7.6) for 1 h at room temperature. Next, the membrane was cut and incubated with 1:5000 diluted monoclonal mouse VDAC1 antibody (abcam, #186321) or 1:1000 diluted monoclonal mouse β-actin antibody (Sigma, A5316) in blocking solution at 4°C overnight mildly shaking. Then membranes were washed three times for 5 min with 0.1% TBS-Tween buffer incubated

Please cite this article in press as: Pilic et al., Hexokinase 1 forms rings that regulate mitochondrial fission during energy stress, Molecular Cell (2024), https://doi.org/10.1016/j.molcel.2024.06.009

with 1:3000 HRP-conjugated secondary anti-mouse antibody for 1 h at room temperature. Washed membranes were incubated with a chemiluminescent reagent (ThermoFisher Scientific) and the signal was captured with ChemiDoc MP Imaging System (Biorad). Relative optical density was determined with Fiji software.

NMR metabolomic profiling

To induce the formation of HK1-rings, cells were cultured in glucose-free DMEM (A14430-01, Gibco) supplemented with 10% FCS, 50 U/mL penicillin-streptomycin, 1.25 μg/mL amphotericin B for 24 h. For NMR flux measurements, the media contained additionally 2 mM ^{13}C-glutamine. NMR sample preparation and analysis were done as previously described.[64] Briefly, cell pellets were mixed with 600 μl methanol (2:1), 200 μl cell supernatants were mixed with 400 μl methanol. Then, samples were lysed using the precellys homogenizer and stored at -20 °C for 1 h until further processing. In the next step, the samples were spun at 10,000 rpm at 4°C for 30 min. The supernatants were lyophilized, and 500 μL of NMR buffer (containing 0.08 M Na_2HPO_4, 5 mM 3-trimethylsilyl propionic acid-2,2,3,3,-d4 sodium salt (TSP) and 0.04 (w/v)% NaN_3 in D_2O, adjusted to 7.4 pH with 8 M HCl and 5 M NaOH) was added to the samples, which were then transferred to 5 mm NMR tubes. All NMR experiments were performed at 310 K on an AVANCE™ Neo Bruker Ultrashield 600 MHz spectrometer equipped with a TXI probe head and processed as previously described.[65] Shortly, the 1D CPMG (Carr-Purcell-Meiboom-Gill) pulse sequence (cpmgpr1d, 512 scans, 73,728 points in F1, 11904.76 HZ spectral width, recycle delays 4 s) with water suppression by pre-saturation was used for 1D ^{1}H NMR experiments. For evaluation of ^{13}C content of analytes ^{13}C-decoupled and non-decoupled ^{1}H 1D CPMG spectra were recorded for each sample. Fraction labeling was calculated using peaks representing protons attached to ^{13}C and ^{12}C (decoupled spectra) and peaks representing protons attached to ^{12}C (non-decoupled spectra). For spectra acquisition, automatic processing (exponential line broadening of 0.3 Hz, phasing and referencing using TSP at 0.0 ppm) Bruker Topspin 4.0.2 software was used. Spectra were imported to Matlab2014b, and the regions around the water, TSP, and remaining methanol signals were excluded. Data analysis and the preparation of figures were carried out in MetaboAnalyst 5.0.

Seahorse measurements

Cells were seeded on XF96 polystyrene cell culture microplates (Agilent, Seahorse) to a confluency of 100%. To induce the formation of HK1-rings, cells were cultured in glucose-free DMEM (A14430-01, Gibco) supplemented with 10% FCS, 50 U/mL penicillin-streptomycin, 1.25 μg/mL amphotericin B for 24 h. Before the measurement cells were washed and incubated in XF assay medium supplemented with 1 mM sodium pyruvate, 2 mM glutamine, and 5.5 mM D-glucose. XF assay medium was not supplemented with glucose for the glucose-free condition. The ratio of oxygen consumption rate (OCR, pmol O_2/min) to extracellular acidification rate (ECAR, mpH/min) was measured with XF96 extracellular flux analyzer (Agilent, Seahorse).

QUANTIFICATION AND STATISTICAL ANALYSIS

Data are presented as mean ± SD, unless otherwise stated. For a two-group comparison paired or unpaired two-tailed t tests were used. For multiple group (>2) comparisons one-way ANOVA was used as followed by indicated post-hoc test to determine *p* values for individual comparisons. No statistical methods were used to predetermine sample size. All statistical analysis was performed using Graphpad Prism 8.0. $p < 0.05$ was considered statistically significant and is presented as * $p < 0.05$, ** $p < 0.01$, *** $p < 0.001$, or **** $p < 0.0001$).